Mina, P., Tsaneva-Atanasova, K., & Bernardo, M. D. (2016). Entrainment and Control of Bacterial Populations: An *in Silico* Study over a Spatially Extended Agent Based Model. *ACS Synthetic Biology*, *5*(7), 639–653. https://doi.org/10.1021/acssynbio.5b00243

Entrainment and control of bacterial populations; an *in silico* approach over a spatially extended agent based model

Petros Mina[1,2*], Krasimira Tsaneva-Atanasova[2,3] Nigel J. Savery[4], Mario di Bernardo[2,5],
1 Bristol Center for Complexity Sciences, University of Bristol, Bristol, United Kingdom
2 Department of Engineering Mathematics, University of Bristol, Bristol, United Kingdom
3 Department of Mathematics, University of Exeter, Bristol, United Kingdom
4 School of Biochemistry, University of Bristol, Bristol, United Kingdom
5 Department of Information and Computer Engineering, University of Naples Federico II, Naples, Italy
∗ **E-mail: Corresponding author petros.mina@bristol.ac.uk, petros@petrosmina.info**

Abstract

As control in cellular populations is becoming more common we extend a spatially explicit agent based model (ABM), developed previously to investigate population emergent behaviour of synchronized oscillating cells in a microfluidic chamber, to include control. Thus, unlike most of the work in models that deal with control of biological systems, we model individual cells with spatial dependencies that may contribute to certain behavioural responses. We use the model to test whether linear control methods can be used to tame the collective behaviour of a bacterial population as recently suggested in the literature. We compare and contrast open and closed loop control in a spatially explicit model of control (specifically proportional control (P-control), proportional-integral control (PI-control) and proportional-integral-derivative control (PID-control) as can be applied in a microfluidic chamber setting) and show when entrainment to a non-natural oscillating period is possible, using an increasing bacterial population size. Results indicate that during open loop control entrainment is only possible in a subset of forcing periods, unlike closed loop control, and a wide variety of dynamical behaviours is obtained outside the regions of entrainment which in a physical setting may be undesirable. However, even with closed loop control, fixed gains cannot harness a population that keeps growing beyond a certain size.

1 Introduction

Control theoretic approaches have been used alongside dynamical models in order to try and tightly regulate (biological) system output. Control theory uses models to describe simple interconnected components to quantify their input and output relationships [1] much like living cells that process information from their surroundings (input) and act upon it (output) [2]. These models usually describe the change of variables with respect to time, i.e. focus on temporal changes, and are used to calculate appropriate actions on the system in order to drive it to a particular state. In cell biology dynamical models of control are more common in the field of neuroscience. In such models, control in the form of external intervention may alleviate symptoms of specific neurological disorders, such as Parkinson's and essential tremors [3–6], for example by disrupting the synchrony of coupled oscillating neurons through electrical stimulation [7–10]. The development of microfluidics technologies over the recent years [11] has allowed researchers to apply control in other cellular systems as well, such as microbe and yeast cells, in order to affect their metabolic states usually by manipulating gene expression. For example Milias-Argeitis *et al.* [12] used a fourth-order linear model describing a light-responsive genetic network in order to control the gene expression of a microbial population, around a reference value, using optogenetics. Uhlendorf *et al.* [13] used a two-variable delay differential equation (DDE) model to capture the dynamics of the yeast hyperosmotic stress response and compute inputs to make a

population of cells to follow a time-varying signal. In Menolascina *et al.* [14], a switching control strategy is developed and implemented in a five-variable time-delayed dynamical system that models a synthetic network in yeast in order to control the output of one of its gene products to a specific value.

However, the study of population-based phenomena under the tightly regulated experimental setups offered by microfluidics technologies [11] suggests that both time and space are of importance in witnessing certain phenomena. In the study of Cho *et al.* [15] the geometry of the cells' surroundings (i.e. the microfluidic chamber) was found to be important for the spatial self-organisation of bacterial colonies. In Prindle *et al.* [16] *E.coli* cells are engineered to display global synchronised oscillations across physically disconnected, yet coupled via gaseous exchange, populations part of a microfluidics platform. The change in the average global frequency of the coupled bacterial colonies [16] was used to detect arsenite in water. Furthermore, the spatial arrangement of the populations was also important to the waveforms witnessed. These examples illustrate that certain behavioural responses are dependent on the synchronisation and spatial distribution of populations, a result also confirmed through theoretical work in reaction-diffusion systems indicating that spatial structure affects qualitative behaviour [17].

Despite the importance of spatial dependence in certain systems, spatial aspects in models of control have not been studied as widely, with limited examples available in the literature. In Hauptmann *et al.* [18] a simplified model of coupled neuronal oscillators uniformly distributed over the area of a circle is studied. Four separate controllers symmetrically arranged at the perimeter of the circle in different quadrants are considered, and each of them may affect the population either locally (local control) or globally (global control) using stimulation proportional to the population average during the previous time (time-delayed feedback). The aim is to study how such control may help disrupt or promote synchrony in the population. Others have focused on continuum type spatial models and how control can be used to obtain specific spatiotemporal patterns. For example, global and local time-delayed control in a 2D-plane is the subject of study in Alhborn and Parlitz [19]. A Ginzburg-Landau partial differential equation (PDE) model is presented [19] and the control aim is to stabilize unstable oscillatory behavior (periodic orbits) or create spatiotemporal chaos using inputs of control found at different locations in the plane. Ghosh [20] investigates control of an activator/inhibitor reaction-diffusion system spatially extended in a 2D-plane and modelled with two PDEs. Global feedback is applied in order to obtain stationary patterns in the plane that can arise from a Hopf-Turing bifurcation mechanism.

We recently developed and studied a spatially explicit model [21] that qualitatively explains the non-trivial spatiotemporal expression patterns seen in the experimental work of Danino *et al.* [22]. In the experimental work [22], a synthetic genetic regulatory network (GRN) based on a quorum sensing (QS) architecture [23] was introduced into *E.coli* cells found within a microfluidic chamber. This GRN had activation-inhibition feedback loops, which lead to oscillatory behaviour [24–29], and also allowed for the production of a small hormone molecule referred to as an autoinducer that was freely exchanged between cells and their environment leading to an all-to-all coupling across members of the population. The result was synchronised population-wide oscillations in the metabolic states of cells, witnessed with the help of green fluorescent protein (GFP) whose induction relied on the GRN dynamics. In the developed ABM [21] cells were considered as agents part of a microfluidic chamber, having explicit spatial positions and whose dynamics were under the influence of the aforementioned GRN. Using the ABM [21] we were able to convincingly illustrate that the oscillations were likely to be an emergent population property, i.e. requiring the presence of more than one cell, and that synchronisation was dependent on the coupling between members of the population, which depends on the cell density, and the concentration and spatial diffusivity of the secreted hormone in the microfluidic chamber. To study the feasibility of linear control techniques over a population of bacterial cells part of a microfluidics platform we extend the spatially resolved ABM presented in Mina *et al.* [21] to study open loop (non-feedback) and closed loop (feedback) control strategies *in silico*. Thus, unlike most work in control of cellular populations [12–14], we also consider the spatial dependencies of coupled cells undergoing global control; in this case classical P-control, PI-control and PID-control [1].

We study the effectiveness and performance of linear control with an increasing population size of 21, 60 and 100 cells where each cell component is modelled with four non-linear ordinary differential equations (ODEs), and subject to control through the manipulation of the small hormone chemical field, modelled with a PDE. Although more cells can be part of the agent-based ODE-PDE model, as shown with the work presented in Mina *et al.* [21], we maintain relatively small-sized populations to reduce the computational cost and thus cover a greater range of values in control parameter space. Specifically, we show when entrainment of the population to a reference sinusoidal signal is possible in open and closed loop control and whether the spatially resolved population can track a time-varying reference signal. Since we use an ABM approach we also study the effect of cell-to-cell heterogeneity across the population, as in a physical setting cell dynamics will tend to vary slightly even between members of the same colony [2, 30, 31]. Hence, the model serves as an *in silico* test-bed where cellular populations are simulated in a spatially explicit 3D-environment and the ability to entrain each population using open and closed loop methods is compared. In addition to demonstrating the efficiency of closed loop over open loop control we uncover the dynamic behaviour of the average population response and how it compares with individual cells part of the model. This approach may serve as a quick and inexpensive way of identifying the most promising strategies to be followed experimentally. Finally, having identified the best performing closed loop controller we simulate a dynamic, motile population where cells can grow, divide and die to evaluate if the performance of a fixed gains controller is affected by the population size.

As in Mina *et al.* [21], we implement the model in BSim [32] an open software platform [33] developed using the Java language [34] to study bacterial populations *in silico*. In order to do so in full, we extend the BSim software [33] by creating methods which can accommodate for the control techniques we are interested in studying. The rest of the manuscript is organised as follows:

- in **section 2**, we revise the original mathematical model presented in Mina *et al.* [21] to include the linear control methods,
- in **section 3**, we present the results obtained from the adapted model and,
- in **section 4**, we conclude with a discussion of results and how they might translate if a physical implementation of the model is considered.

Additional material with regards to the computational implementation of the model in BSim [32, 33] and the post-processing of results may be found in the supplementary material that accompanies this manuscript.

2 The spatiotemporal model with control

In the experimental work of Danino *et al.* [22] a GRN comprised of three genes was introduced into bacterial cells and allowed for oscillations to exist due to the presence of activation-inhibition feedback loops part of the GRN [21, 24–29]. As shown in **figure 1** these genes are, *luxI*, *aiiA* and *yemGFP* and all are under the influence of the same promoter, *li-P* [22]. The genes have a C-terminal degradation tag sequence that shortens the half-life of their protein products considerably [35] and are introduced into bacteria on separate plasmids [22]. The *luxI* gene encodes for the LuxI synthase (LI), a protein that produces acyl homoserine lactone (AHL). AHL, also known as an autoinducer, can interact with the constitutively expressed protein LuxR, the AHL autoinducer receptor (LR), to form the LuxR:AHL complex (L:A) and activate the promoter *li-P*, allowing for the transcription of all three genes [22]. The AHL molecule is removed from the system by interacting with the acyl homoserine lactonase (aA) enzyme that degrades AHL. AHL can also freely diffuse across the cell membrane allowing for communication and hence coupling between all cells in the population [22]. It is to be noted that in

equations and figures the AHL autoinducer is abbreviated to the variables A (for intracellular AHL) and $\tilde{\text{A}}$ (for extracellular AHL). The AHL abbreviation is only used within the text. Thus, the following chemical interactions are assumed to occur within each cell:

$$\text{LI} \xrightarrow{k_{p2}} \text{A}, \tag{1}$$

$$\text{A} + \text{aA} \underset{k_{r2\_}}{\overset{k_{r2\_+}}{\rightleftharpoons}} \text{A:aA} \xrightarrow{k_{cat}} \text{aA} + \text{P}, \tag{2}$$

$$\text{A} + \text{LR} \underset{k_{r1\_}}{\overset{k_{r1\_+}}{\rightleftharpoons}} \text{L:A}, \tag{3}$$

where LI, A, aA, LR and L:A are the LuxI protein, the AHL molecule, the acyl homoserine lactonase enzyme aiiA, the LuxR protein and the LuxR:AHL transcription factor. A:aA is an intermediate complex formed between the AHL autoinducer (A) and the autoinducer degrading enzyme aiiA (aA). Reaction rates are described with the parameters k_x. P is simply the product of AHL degradation and is not involved in further reactions that can affect network dynamics.

Thus, the internal metabolic states of each cell, as a result of the GRN, can be modelled with:

$$\frac{d[\text{LI}]_i}{dt} = a_{0_L} + k_{p_{LI}} \frac{[\text{L:A}]_i^2(t)}{K_{m_{LA}}^2 + [\text{L:A}]_i^2(t)} - \frac{\delta_1 [\text{LI}]_i(t)}{f\Big([\text{LI}]_i(t) + [\text{aA}]_i(t)\Big) + 1}, \tag{4}$$

$$\begin{aligned}\frac{d[\text{A}]_i}{dt} =& k_{p2}[\text{LI}]_i(t) - \left(k_{r1+}([\text{L}_{\text{TOT}}] - [\text{L:A}]_i(t)) + \frac{k_{cat_{aA}}[\text{aA}]_i(t)}{K_{m_{aA}} + [\text{A}]_i(t)} + \tau_A\right)[\text{A}]_i(t) \\ &+ k_{r1\_}[\text{L:A}]_i(t) - \eta_{\text{cell}}\left([\text{A}]_i(t) - [\tilde{\text{A}}](t)\right),\end{aligned} \tag{5}$$

$$\frac{d[\text{aA}]_i}{dt} = a_{0_A} + k_{p_{aA}} \frac{[\text{L:A}]_i^2(t)}{K_{m_{LA}}^2 + [\text{L:A}]_i^2(t)} - \frac{\delta_2 [\text{aA}]_i(t)}{f\Big([\text{LI}]_i(t) + [\text{aA}]_i(t)\Big) + 1}, \tag{6}$$

$$\frac{d[\text{L:A}]_i}{dt} = k_{r1+}\Big([\text{L}_{\text{TOT}}] - [\text{L:A}]_i(t)\Big)[\text{A}]_i(t) - k_{r1\_}[\text{L:A}]_i(t) - \tau_{LA}[\text{L:A}]_i(t), \tag{7}$$

where $[\text{LI}]_i$, $[\text{A}]_i$, $[\text{aA}]_i$ and $[\text{L:A}]_i$ are variables describing the concentration of LuxI, intracellular AHL, acyl homoserine lactonase, and the LuxR:AHL complex respectively of the i-th cell in the population. A detailed derivation of this model is given in the supplementary information of Mina *et al.* [21]. Values of all parameters are given in **table S1** in the supplementary information accompanying this manuscript.

Proteins that are produced directly from the genetic network (LI and aA) are described with two types of production rates, a basal rate a_{0_X}, and Hill functions with production rates k_{p_X} with Hill coefficient two (where X is any protein). Molecules not produced directly from the genetic network are involved in linear reactions proportional to their concentration with rates $k_{r-/+}$ and also follow first order degradation kinetics with rate τ_X with the exception of AHL (A) that undergoes enzymatic degradation with rate $k_{cat_{aA}}$ represented by a Michaelis-Menten function. The concentration of free LuxR is obtained by subtracting the concentration of the LuxR:AHL (L:A) complex from the total

concentration of LuxR, L_{TOT}. The autoinducer molecule diffuses in and out of the cell depending on the intracellular and extracellular concentration difference with a rate $\eta_{\text{cell}}(\equiv \frac{A_{\text{cell}} \times D_m}{V_{\text{cell}}})$, where A_{cell} is the surface area of the cell, D_m the membrane permeability coefficient and V_{cell} the volume of an *E.coli* cell, as in Garcia-Ojalvo *et al.* [36]. The terms at the end of equations (4) and (6) describe the enzymatic degradation of LI and aA respectively by the protease ClpX/P due to the presence of the aforementioned C-terminal degradation tags [22,37]. The parameters δ_1 and δ_2 incorporate the maximum catalytic rate ($V_{\max}$) multiplied by the total ClpX/P concentration. The entire term is normalised by the Michaelis-Menten constant of enzyme ClpX/P ($K_{M_{\text{clx}}}$) for LI and aA respectively. The parameter f is the inverse of the Michaelis-Menten constant of ClpX/P, $f = 1/K_{M_{\text{clx}}}$.

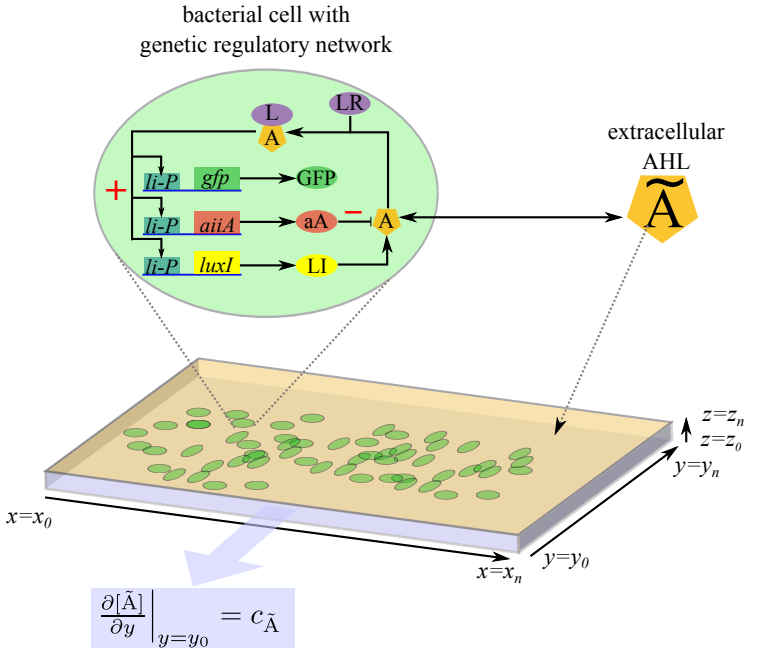

Figure 1. The microfluidic chamber and the quorum sensing regulatory network of Danino *et al.* [22]. Cells (green ellipses) are found inside a one cell thick microfluidic chamber defined by the (x, y, z) dimensions such that $x \in [x_0, x_n]$, $y \in [y_0, y_n]$ and $z \in [z_0, z_n]$ as illustrated in the figure. Each cell carries a GRN composed of three genes. The *luxI* gene encodes for the LuxI enzyme (LI-yellow), which produces the molecule acyl homoserine lactone (abbreviated as AHL in the main text and presented as variable A, with orange color, in the figure). AHL combines with the constitutively expressed LuxR (purple), to form a complex, L:A, that can activate the promoter *li-P* (blue). This drives the expression of all three genes, *gfp*, *aiiA* and *luxI*. AHL (A) is removed from the system by enzymatic degradation catalysed by the aA enzyme (aA-red). Positive and negative feedbacks steps within this network are indicated with a red plus/minus sign respectively. AHL can also freely diffuse through the cell membrane. The extracellular concentration of AHL is labelled as $\tilde{A}$ in the figure. Boundary conditions are such that extracellular AHL, $\tilde{A}$, can escape from the microfluidic chamber exit at a rate $c_{\tilde{A}}$, $\frac{\partial[\tilde{A}]}{\partial y}\Big|_{y=y_0} = c_{\tilde{A}}$.

To remain consistent with the experimental setup of Danino *et al.* [22] we define a three dimensional coordinate system, the (x, y, z)-plane, where $x \in [x_0, x_n]$, $y \in [y_0, y_n]$ and $z \in [z_0, z_n]$. The subscript n in the axes coordinates represents the maximum distance of each coordinate from the origin, labelled with the subscript 0, in micrometers. As illustrated in **figure 1** this defines the boundaries of the microfluidic chamber. We set $z_0 = 0$ and $z_n = 1$ to model a one cell thick microfluidic chamber as in Danino *et*

al. [22] thus we can restrict ourselves to spatial coordinates on a two-dimensional plane (here the x and y coordinates). Thus, the concentration of external AHL is described using the reaction-diffusion PDE:

$$\frac{\partial\ [\tilde{\mathrm{A}}](x,y,t)}{\partial t} = \underbrace{D_{\tilde{\mathrm{A}}}\nabla^2[\tilde{\mathrm{A}}](x,y,t)}_{\text{brownian diffusion}} + \underbrace{\sum_{i=0}^{N}\eta_{\text{env}}([\mathrm{A}]_i(t) - [\tilde{\mathrm{A}}](x,y,t))}_{\text{AHL exchange}} - \underbrace{\tau_{\tilde{\mathrm{A}}}[\tilde{\mathrm{A}}](x,y,t)}_{\text{degradation}}, \tag{8}$$

where $D_{\tilde{A}}$ is the Brownian diffusion coefficient of extracellular AHL, η_{env} describes the diffusion of AHL across each cell's membrane (each cell denoted with the index i and N cells are part of the model) and also adjusts the concentration of extracellular AHL dependent on the microfluidic chamber's volume, V_{env}, such that $\eta_{\text{env}} = \eta_{\text{cell}}/V_{\text{env}}$. The boundary conditions for this PDE are such that extracellular AHL can escape the microfluidic chamber exit which in this model is located, at the xz-plane, such that $\frac{\partial[\tilde{\mathrm{A}}]}{\partial y}\Big|_{y=y_0} = c_{\tilde{\mathrm{A}}}$, as shown in **figure 1**. As with the experiments of Danino *et al.* [22] a $200 \times 50 \times 1\ \mu\text{m}^3$ microfluidic chamber is modelled.

Our aim is to control the output of a population of cells whose metabolic states undergo oscillations [21, 22] to a reference signal, $r(t)$, using a controller setup like the one illustrated in **figure 2**. As was shown in Mina *et al.* [21], the state of the cells is affected by the availability of external AHL thus the action of the controller setup is to modify the concentration of external AHL in the microfluidic chamber in an effort to control the cell state. The controller receives feedback from the cells found in the microfluidic chamber using optical readers and calculates the amount of AHL to be supplied to the chamber in order to make cells follow the reference value $r(t)$.

There is no direct measure of the intracellular concentrations (i.e. the system output) and in the experimental setup the state of the system would be inferred from the output of GFP whose induction relies on the GRN dynamics [22]. The population fluorescence and cell density is obtained from measurements supplied by the fluorescence and optical density meter respectively. These measurements can be used to calculate the average concentration of GFP, $\widehat{[\mathrm{GFP}]}$, as shown in Canton *et al.* [38]. The difference between $\widehat{[\mathrm{GFP}]}$ and the reference value, $r(t)$, is the instantaneous error, $e(t)$. The instantaneous error is used by the controller to calculate the amount of external AHL to be supplied or removed from the chamber according to proportional, integral and derivative control. In the case of open-loop control the constant feedback provided by the optical readers of the setup is not used to update the action of the controller and the value $r(t)$ is used directly as the amount to be provided as influx into the microfluidic chamber. Additional details of the implementation of control in the BSim environment are given in the supplementary information that accompanies this manuscript.

For simplicity, in our model, we assume that GFP follows the dynamics of LI and we use LI as our reference read-out of the system. Thus we define the standard error between the signal's reference value and the system's current state as:

$$e(t) = r(t) - \widehat{[\mathrm{LI}]}(t) \tag{9}$$

where $\widehat{[\mathrm{LI}]}(t) = \frac{1}{N}\sum_i^N [\mathrm{LI}]_i(t)$ is the average concentration of LI of a population of size N and $r(t)$ is the reference signal.

We investigate three types of reference signals, a constant reference value, $r_{\text{c}}(t)$, a sinusoidal function, $r_{\text{sin}}(t)$, and a trapezoidal (ramp) function, $r_{\text{rmp}}(t)$. The constant reference signal, $r_{\text{c}}(t)$, and the sinusoidal reference signal, $r_{\text{sin}}(t)$, are given by the equations:

$$r_{\mathrm{c}}(t) = \begin{cases} 0, & t < t_s \\ c, & t_s \leq t < t_e \\ 0, & t \geq t_e \end{cases} \tag{10}$$

and

$$r_{\sin}(t) = \begin{cases} 0, & t < t_s \\ c + \alpha \sin\left(\frac{2\pi t}{T_f}\right), & t_s \leq t < t_e \\ 0, & t \geq t_e \end{cases} \tag{11}$$

where c is the constant offset from zero, 2α is the amplitude of the sine wave (i.e the length between the peak found at $c+\alpha$ and the trough found at $c-\alpha$), T_f the forcing period and t_s, t_e the signal start and signal end times respectively.

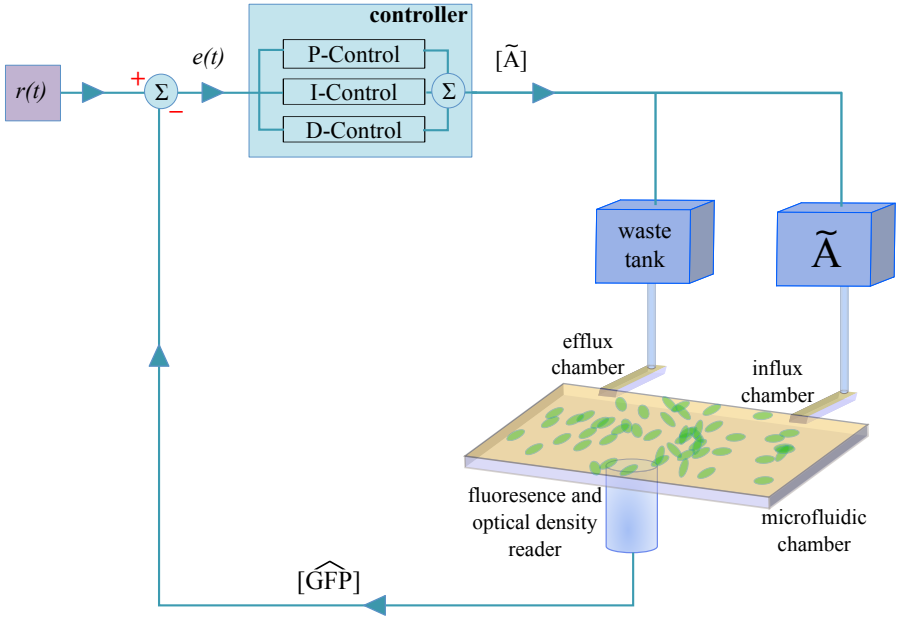

Figure 2. Schematic of an idealised controller apparatus for implementing control over a population of cells in a microfluidic chamber. The fluorescence and optical density meters are used to measure the population fluorescence and cell density whose values are used to estimate the average concentration of GFP ($\widehat{[\mathrm{GFP}]}$) in the population [38]. The controller calculates the instantaneous error, $e(t)$, using $\widehat{[\mathrm{GFP}]}$ and the current value of the reference signal, $r(t)$. For closed loop control, the instantaneous error is used to calculate the modulation of external AHL required in the chamber according to proportional (P), integral (I) and derivative (D) control. The modulation is accomplished using micropipettes found between the influx and efflux chambers and the respective chemical ($\tilde{\mathrm{A}}$) and waste tanks as shown in the figure. For open loop control the feedback connection between the chamber and the controller is overridden and the value $r(t)$ is used directly for controller actuation.

Given the height of the ramp function, $h = y_{\max} - y_{\min}$, such that $y_{\max}$ and $y_{\min}$ are the values of the two ramp bases, t_1 the time the reference signal reaches $y_{\max}$ and t_2 the time of descent from $y_{\max}$ back to $y_{\min}$, we can construct the ramp function with the discontinuous equation:

$$r_{\text{rmp}}(t) = \begin{cases} y_{\min}, & t < t_s \\ c_{r1} + m_1 t, & t_s \leq t < t_1 \\ y_{\max}, & t_1 \leq t < t_2 \\ c_{r2} + m_2 t, & t_2 \leq t < t_e \\ y_{\min}, & t \geq t_e \end{cases} \tag{12}$$

where $m_1 = \frac{y_{\max} - y_{\min}}{t_1 - t_s}$, $m_2 = \frac{y_{\min} - y_{\max}}{t_e - t_2}$, $c_{r1} = y_{\min} - m_1 t_s$ and $c_{r2} = y_{\max} - m_2 t_2$ are gradients and intercept values that define the two ramp legs as straight lines. The three reference signals are presented in **figure 3**. In the case of the periodic reference signal, $r_{\sin}(t)$, we consider the population to be entrained when the average period of the entire population is equal to the forcing period, T_f. The periodic behaviour of the population is assessed using Poincare sections, as described in the supplementary information.

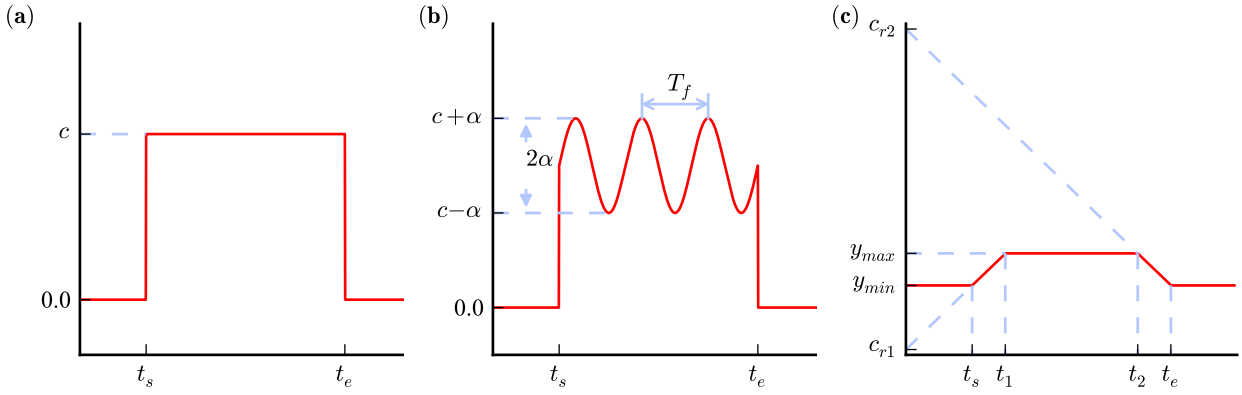

Figure 3. The reference signals used for entrainment and tracking of the bacterial population. The y-axis refers to the values of desired cell state (i.e. intracellular concentration of a protein variable) and the x-axis represents time. The reference signal is switched on at time t_s and switched off at time t_e. The population is made to follow **(a)** a fixed reference value c (equation (10)), **(b)** a sinusoidal signal with period T_f (equation (11)) and **(c)** a ramp of height $h = y_{\max} - y_{\min}$ (equation (12)).

2.1 Open loop control

Open loop control is implemented by modulation of the concentration of the external autoinducer chemical field, $[\tilde{\text{A}}]$, using the time-varying input, $r_{\sin}(t)$ (equation (11)). Specifically, the external chemical field equation becomes:

$$\frac{\partial\,[\tilde{\text{A}}](x,y,t)}{\partial t} = D_{\tilde{\text{A}}}\nabla^2[\tilde{\text{A}}](x,y,t) + \sum_{i=0}^{N} \eta_{env}\left([\text{A}]_i(t) - [\tilde{\text{A}}](x,y,t)\right) - \tau_{\tilde{\text{A}}}[\tilde{\text{A}}](x,y,t) + k_{\text{o}} r_{\sin}(t), \tag{13}$$

where k_o, the open loop gain, is set to one and we vary the values α and c of $r_{\sin}$. Microfluidic setups can allow for such modulation as illustrated in Mondragon *et al.* [39] where the flow of the inducer molecule through the chamber is adjusted to follow a sinusoidal time-varying signal.

2.2 Closed loop control

In contrast to open loop control, closed loop control continually adjusts the input to the system based on feedback from the system's current state. We implement P-control, PI-control and PID-control. For this we adjust the external chemical field equation for control as follows:

$$\begin{aligned}\frac{\partial\,[\tilde{\mathrm{A}}](x,y,t)}{\partial t} =& D_{\tilde{\mathrm{A}}}\nabla^2[\tilde{\mathrm{A}}](x,y,t) + \sum_{i=0}^{N}\eta_{env}\left([\mathrm{A}]_i(t) - [\tilde{\mathrm{A}}](x,y,t)\right) - \tau_{\tilde{\mathrm{A}}}[\tilde{\mathrm{A}}](x,y,t) \\ & \underbrace{\underbrace{+k_p e(t)}_{\text{P-control}} + k_I\int_0^t e(\tau)d\tau}_{\text{PI-control}} + k_D\frac{de(t)}{dt} \\ & \underbrace{\qquad\qquad\qquad\qquad\qquad\qquad}_{\text{PID-control}}\end{aligned} \tag{14}$$

where k_p, k_I and k_D are the gains for the proportional, integral and derivative controllers respectively and $e(t)$ is the instantaneous error defined in equation (9). Setting k_D to zero allows us to investigate PI-control only and setting both k_D and k_I to zero allows us to investigate P-control only.

2.3 Modelling a growing population

Depending on the surrounding environmental conditions *E.coli* cells will have a mean doubling time ranging from approximately 30 minutes (in a nutrient-rich medium) to several hours (in a poor-nutrient medium) [40]. Since nutrients will not be a limiting factor in a tightly regulated microfluidic setup [22,41] we assume that cell-division time will be closer to 30 minutes rather than several hours and set the cell doubling time to 40 minutes. To avoid synchronous cell division we model the cell growth rate with a Gaussian of mean doubling time of 40 minutes and a standard deviation of 4 minutes. For the internal variables (LI, AHL, aA and LA), daughter cells assume the concentration values of their parent cell. We further assume that the maximum population size will be limited only by the dimensions of the microfluidic chamber. This is consistent with the experimental setup of Danino *et al.* [22] since cells that reach the chamber exit are eventually cleared away from the chamber. As such, the maximum theoretical population size is 10000 cells (assuming a $200\times50\times1$ $\mu\mathrm{m}^3$ chamber and cells with radius of 1 $\mu\mathrm{m}^3$). Of course cells may die before reaching the chamber exit. Hence, we model cell death by randomly choosing cells to be removed from the simulation once the maximum population size has been reached, using a uniform distribution. We remove as many cells necessary to accommodate the newly born daughter cells without exceeding the maximum population size. Thus, during the simulation the population may only grow up to the maximum specified size but individual cells will keep undergoing cell division (if alive) and cell death.

3 Results

3.1 Open loop

We investigate the feasibility to control an increasing population size *in silico* using a non-feedback mechanism by modelling a static (non-dividing) population. We first start by investigating the controllability of a single cell and then move to bigger size populations of 21, 60 and 100 cells. There are three

control parameters to be investigated in open loop control (equation (13)), as given by $r_{\sin}(t)$ (equation (11)); the constant offset c, the amplitude α and the period of the forcing T_f. We note that the system's period changes when it is forced with just a constant value, say c (i.e by supplying a constant amount of AHL in the chamber for all time). We call the period that the system assumes under this constant forcing to be the natural period, T_n. A single cell could be entrained to an external period away from T_n by forcing it with $r_{\sin}(t)$ characterized by minimal values for α and c so we direct the focus of the research to the bigger population sizes. We first investigate the effect of varying parameter c by fixing the external force frequency T_f at a value away from the unforced natural period of the cell population ($T_f = 15000$ sec). As can be seen in the example of 60 cells shown in **figure 4 (a)** the population is entrained completely above a certain threshold for c even for small values of the amplitude, α. The value of c that this occurs at increases with increasing population size (results not shown). For each investigated population we fix c at a value lower than this threshold to investigate the effects of varying the forcing period, T_f, and amplitude, α. The values of the control parameters used are given in the respective figures where results are illustrated and in the main text where results are described.

As shown in **figure 4 (b)**, for a population of 21 cells, variation of the two parameters of amplitude and period (α, T_f) shows regions of entrainment in the $(T_f/T_n, \alpha)$-plane, close to multiples of the natural period, T_n. The value of the natural period, T_n, for a 21 cell population is approximately 368 min ($c = 1.0$). The increasing value of the amplitude α allows the system to be entrained to the forcing period even at values away from the natural frequency T_n, a behaviour typical of two distinct coupled oscillators [42]. Note that near $T_f/T_n \approx 1$ minimal amplitude, α, of the external input is sufficient to entrain the population. This is best illustrated in **supplementary figure S3** where α is fixed at 0.2 for a population of 21 cells and T_f is varied in small increments. As illustrated in **figure 4 (b)**, above a certain amplitude threshold near $T_f/T_n \approx 2$ the population is again synchronised to the external forcing period. Phase diagrams of the system in the ([aA],[LI])-plane constructed from stroboscopic sections of the system's output illustrate the presence of quasi-periodic oscillations outside the entrained regions whilst a limit cycle exists within the entrained regions (see **supplementary figure S4**).

The same features observed in populations of 21 cells are also detected when larger populations are simulated. Qualitatively similar diagrams of the $(\alpha, T_f/T_n)$-plane for both 60 and 100 cells are shown in the **supplementary figure S5** where broad areas of entrainment near the natural period of the cell population can be seen. This natural period is approximately 360 minutes for both 60 and 100 cell populations ($c = 3.2$ and 5.0 respectively).

We also investigate the effect of heterogeneity in a population of 60 cells by varying the production and degradation rates of each cell part of the population using a Gaussian distribution for each of the parameters (δ_1, δ_2, τ_A, τ_{LA}, $k_{p_{LI}}$, $k_{p_{aA}}$, a_{0_L}, a_{0_A}). The mean of each distribution assumes the value of the respective parameter as given in **table S1** in the supplementary information and standard deviation is a percentage of this value. Specifically, we use standard deviations of 2%, 4% and 6% of the mean value of each parameter. As shown in the **supplementary figure S7**, in the absence of heterogeneity all cells in the population oscillate with the same amplitude, constant offset and period, effectively responding to the forcing period in unison. However, as seen in **figure 5**, as heterogeneity is increased in the population cells start to lose their in-unison effect and each cell in the population starts to oscillate with slightly different amplitude and constant offset values. This becomes more pronounced at higher variability (6%) where the population may be entrained, whereas with lower variability for the same control parameter values (T_f, c, α) is not, but cells no longer have an equal output. In general the increased level of heterogeneity decreases the average amplitude of the population oscillatory behaviour and creates a range of constant offset and amplitude values for the oscillating population as illustrated by the histograms presented in **figure 5**.

The ABM also captures a variety of dynamical behaviours as illustrated in **figure 6**, where we present the average response of a population with 2% heterogeneity when subject to entrainment during open loop control. Note that similar entrainment areas exist as with the homogeneous population presented

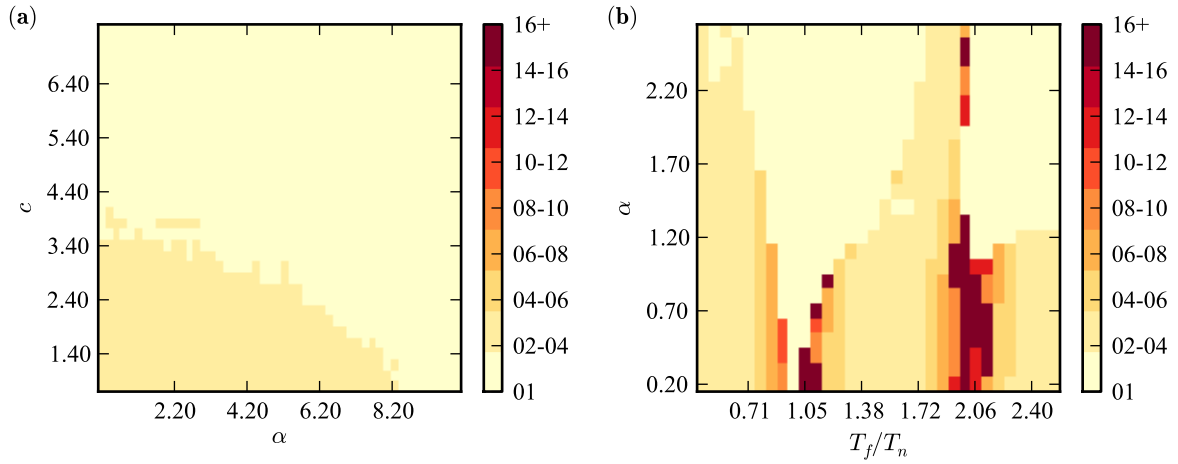

Figure 4. Average behaviour of homogeneous cell populations under open loop control. The ABM illustrates a wide range of dynamic behaviour when forcing the oscillating population during open loop control (equation (13)) according to the three parameters, c, α, T_f of $r_{\sin}(t)$ (equation (11)). Each color pixel of the presented planes illustrates the periodic behaviour of the population average. The value of the periodic output is given as multiples of the forcing period and is illustrated in the colorbar. **(a)** The effect of increasing the constant offset, c, in open loop control (population of 60 cells, $T_f = 15000$ sec). Above a certain value for c the population is completely entrained for all amplitude values, α. This threshold increases with increasing population size. **(b)** The $(\alpha, T_f/T_n)$-plane presented above shows the periodic output a homogeneous population that is 21 cells strong ($c = 1.0$). Areas of entrainment appear at multiples of the natural period, $T_f/T_n \approx 1$ and $T_f/T_n \approx 2$. High periodic behaviour is seen before and after regions of entrainment. Similar behaviour is also seen in bigger sized populations as illustrated in the **supplementary figure S5**.

in **figure 4**. The points labelled 1–6 in **figure 6** illustrate the average population response of the system dynamics and are expanded in the respective sub-panels showing the time-series and associated Poincare (stroboscopic) sections. At point one on the far left of the $(\alpha, T_f/Tn)$-plane presented in **figure 6** there is periodic behaviour on a torus governed by two periods (period-2 and period-30). As the forcing value approaches the region of entrainment the output becomes high-periodic and only dominated by a single-period as shown by sub-panel two. Entrainment is illustrated in sub-panel three. The behaviour illustrated in sub-panels four and five is similar to that of sub-panels two and three respectively. The torus behaviour governed by the two distinct periods (shown in sub-panels 1 and 4 of **figure 6**) is also sensitive to amplitude variation. For example going from point 1 to point 6 on the $(\alpha, T_f/Tn)$-plane removes the high period that underlines the dynamics of point 1. At point 6 only the period-2 remains as illustrated in the power spectrums presented in **figure S6**.

3.2 Closed loop

As seen by our model results, open loop control can only entrain a bacterial population within a limited range of control parameter values, namely the amplitude and forcing period parameters α and T_f respectively. Furthermore, increasing variability in the population causes cells to lose their clustering effect. Thus, we proceed to check whether closed loop control performs better in regulating the output of a population of oscillating cells.

To test the ability to entrain the population over a range of periodic inputs we simulated a homogeneous population of 21 cells under the influence of P-control. We varied the amplitude and period of

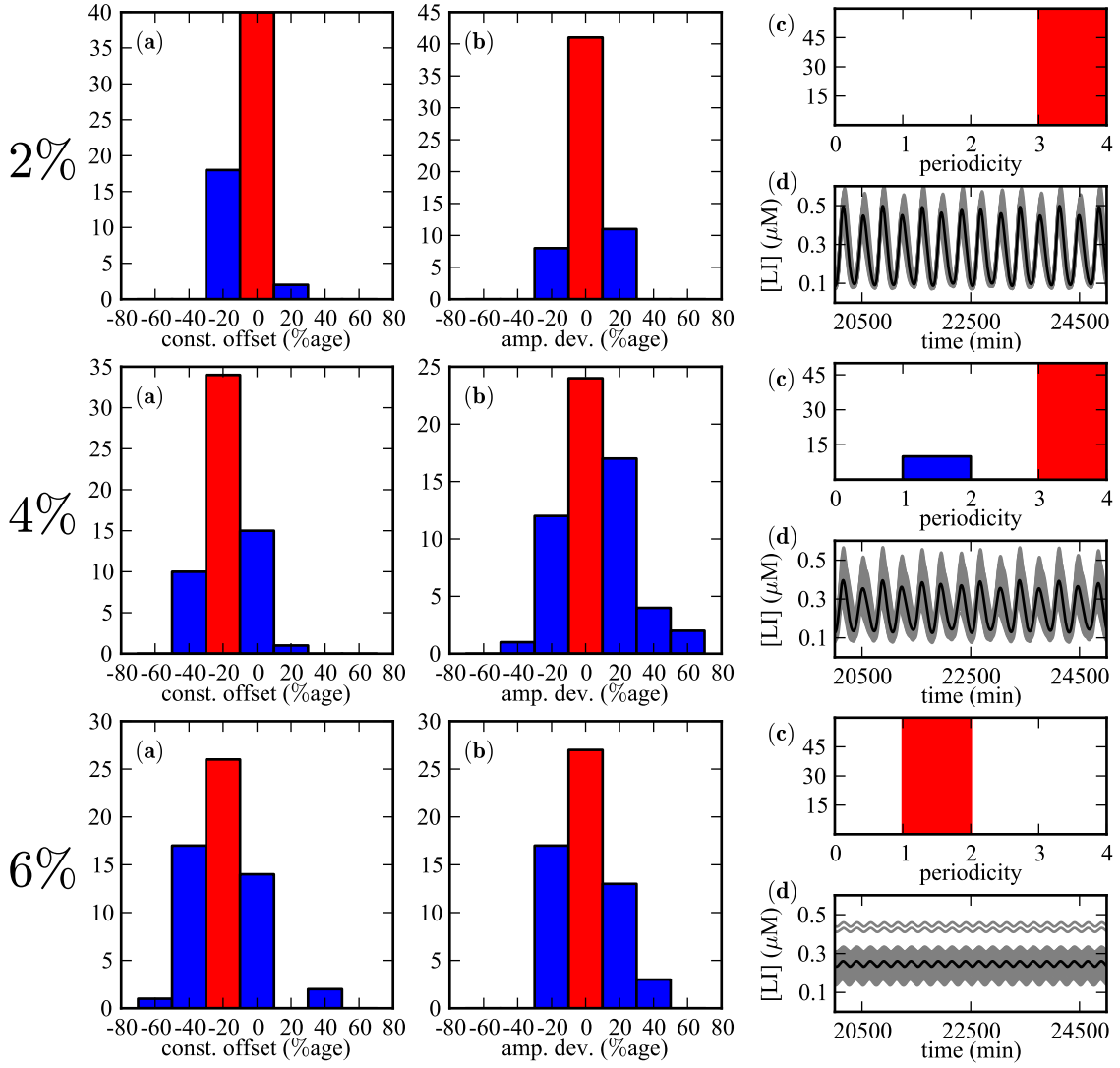

Figure 5. The effect of heterogeneity on a 60-cell population during open loop control. The introduction of heterogeneity in the population through parameter variation, as described in the main text, reduces the clustering effect of a population subject to forcing ($T_f = 15000$ sec, $c = 3.0$, $\alpha = 1.0$) as seen through variability of oscillatory output in the **(a)** constant offset and **(b)** amplitude of cells part of the population, given as a percentage deviation from the homogeneous case. **(c)** Periodicity of cells in the population. **(d)** Time-series of the entire population (grey) is compared with the population average response (black line). In the histograms (a)-(c), the y-axis represents the number of cells and the red column illustrates the population mode. The population response in the absence of heterogeneity, i.e. the 0% case, may be found in the **supplementary figure S7**.

the reference signal $r_{\sin}(t)$, parameters α and T_f in equation (11), to match the values of the $(\alpha, T_f/T_n)$-plane presented in **figure 4 (b)**. The constant offset, c, was fixed at the same value as for the open loop control of this population size ($c = 1.0$). As shown in **figure 7**, P-control can entrain the population over all amplitude and period values.

Furthermore, we assess the effect of the closed loop controller (P-control) with increasing levels of heterogeneity, as we did with open loop control. **Figure 8** shows the population response when 2%, 4% and 6% heterogeneity is introduced in the population. The homogeneous case, i.e. 0% heterogeneity, is given in the **supplementary figure S8**. As seen when comparing **figure 8** with **figure 5** the closed

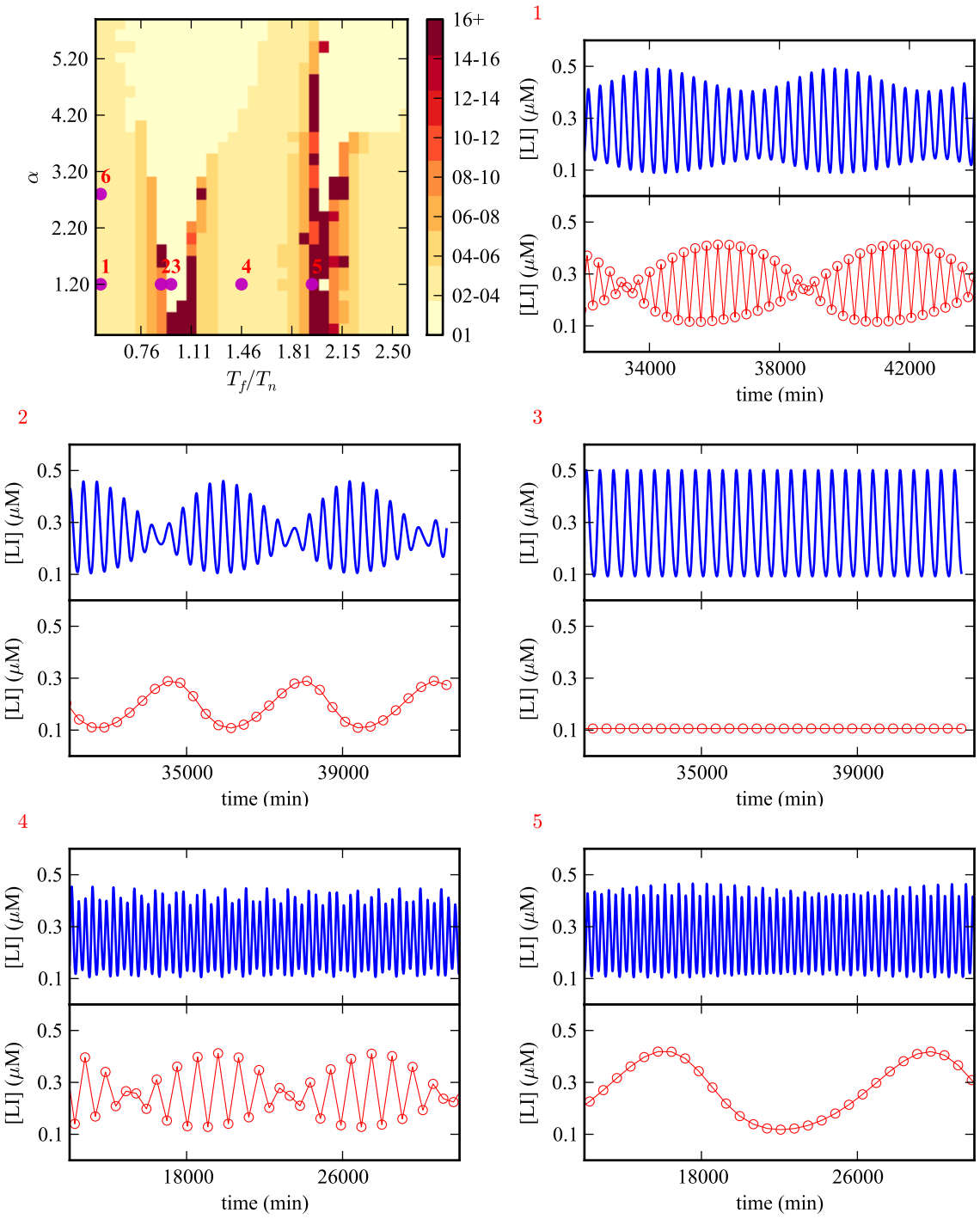

Figure 6. Average behaviour of a 60-cell heterogeneous population during open loop control. Heterogeneity at 2%. The agent based model illustrates a wide range of dynamic behaviour that can be seen when trying to entrain the oscillating population to the forcing period when we vary the amplitude, α, and force period, T_f. The $(\alpha, T_f/T_n)$-plane presented illustrates the periodic output of the population average response. The average behaviour of the population in the annotated segments of the plane is presented in the panels that follow. These show the time-series of the output (top panels) and the Poincare (stroboscopic) sections (bottom panels) that result from strobing the output with the forcing period T_f. Details are given in the main text.

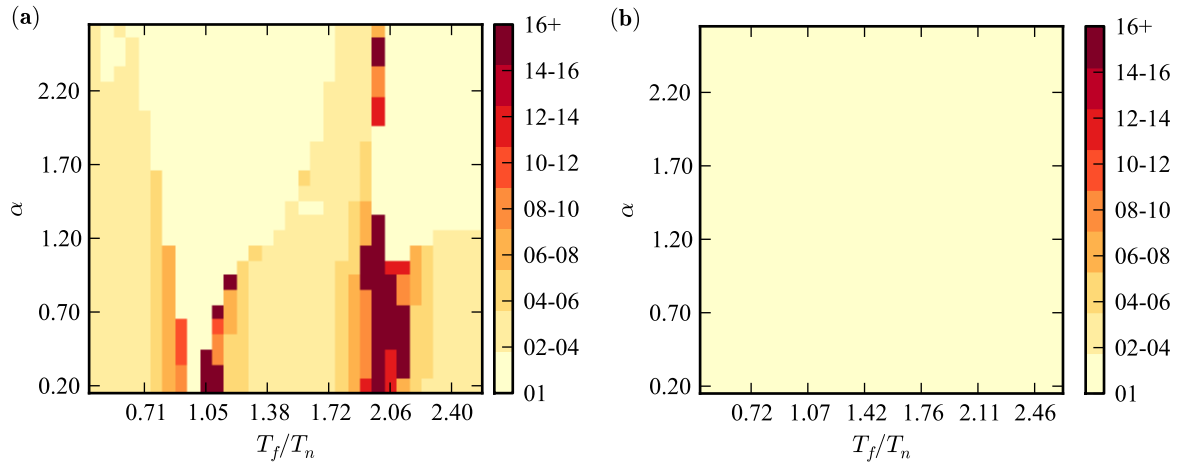

Figure 7. Open vs closed loop entrainment for a homogeneous population of 21 cells. P-control (right panel, $k_p = 500$) can entrain a population of 21 cells for all periodic signals whilst open loop control (left panel) can only entrain the population near multiples of natural frequencies.

loop controller performs better than the open loop control system by minimising the variability of the population in terms of amplitude and constant offset. In addition to this the closed loop control system does not reduce the average amplitude of the population, as opposed to the open loop controller. We also note that the closed loop controller manages to maintain the mode of the population in terms of constant offset and amplitude for all levels of heterogeneity. That is, the population mode of both constant offset and amplitude is the same as the homogeneous population (presented in **figure S8**), unlike the open loop results.

In addition to the sinusoidal reference signal, $r_{\sin}$ (equation (11)), we also test the ability to control a 21, 60 and 100 cell heterogeneous population (heterogeneity at 2%) with the closed loop control methods. Specifically, we use a fixed value reference signal (r_c, equation (10)) and a time varying signal, a ramp (r_{rmp}, equation (12)). Cells are subjected to P-control using three reference signals; a fixed value, a trapezoidal shaped ramp and a sinusoidal signal. With P-control the population average and reference value maintain a standard error difference, for all population sizes modelled. An example of the response of a 60 cell population is shown in **figure 9**.

To try and minimise the standard error we introduced integral and derivative action to the control scheme. An example of the response of a 60 cell heterogeneous population for the fixed reference signal, r_c, undergoing PI-control and PID-control is presented in **figure 10**. PI-control minimises the standard error to 1.47%, as opposed to 28.2% with P-control only, but further improvement results to small amplitude oscillations around the reference value as illustrated in **figure 10 (a)**. PID-control, shown in **figure 10 (b)**, can reach 93% of the reference value (i.e. 1.4 μM when the reference value is 1.5 μM) in less than 48 hours ($\approx$ 46.5 hours) and also minimises the standard error to 0.33% of the reference value. The PID-controller has an improved response time over PI-control. Specifically for the 60-cell example illustrated in **figure 10** PI-control has a settling time, the time needed to reach the peak value (the maximum value the population assumes with PI-control is 1.47 μM), of $\approx$ 1550 hours whilst PID-control can reach the same value in $\approx$ 245 hours and has a settling time of $\approx$ 737 hours (the maximum value the population assumes with PID-control is 1.495 μM).

As seen, PID-control has had the best performing control strategy in terms of the population's settling time and also in minimising the standard error. However, in a physical setting the population will keep growing through cell division to fill-up the chamber, and not remain static as with the modelled population sizes. Also, some of the population members will undergo cell death. It is not unlikely that

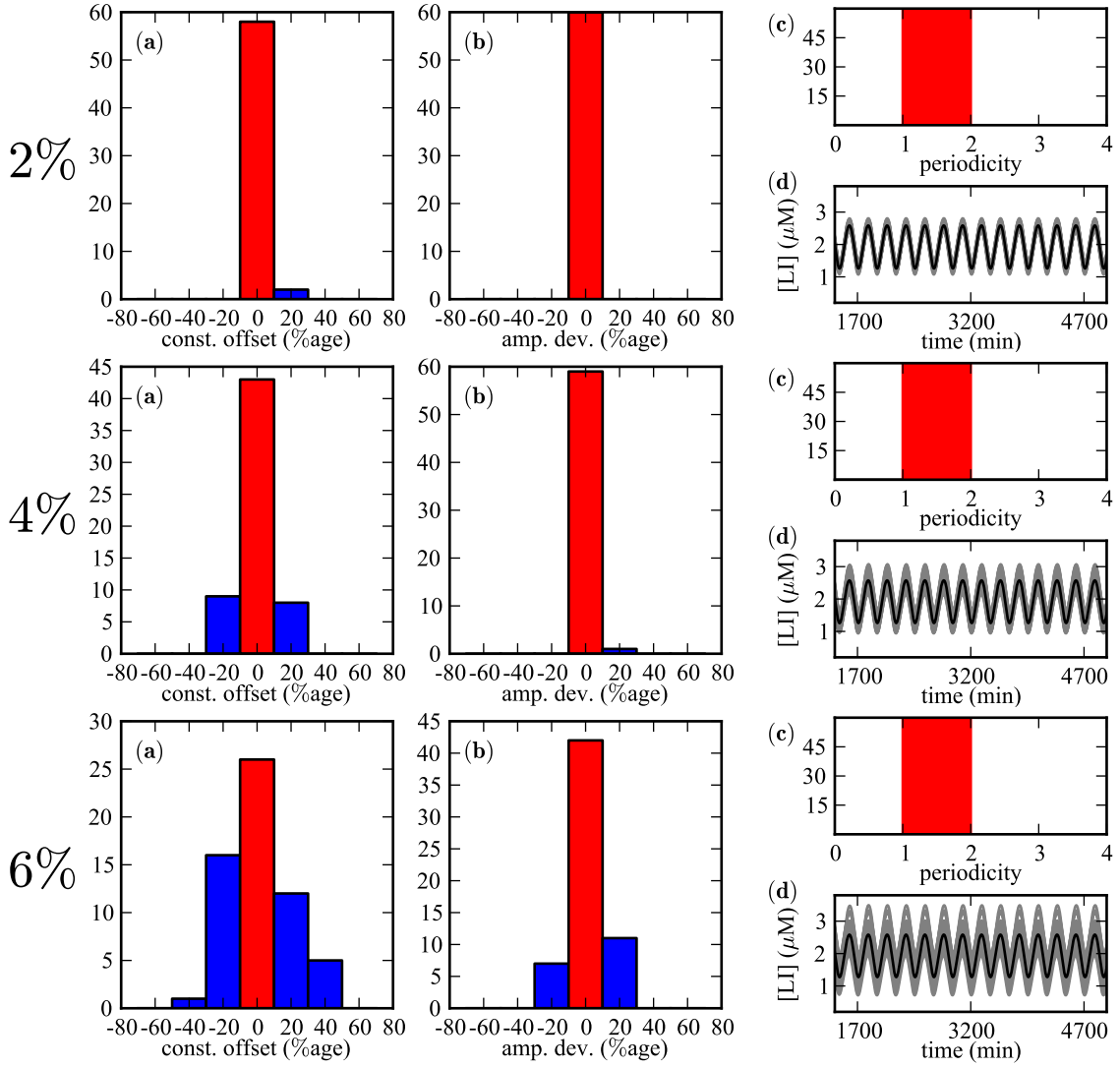

Figure 8. The effect of heterogeneity on a 60-cell population during P-control. The closed loop controller minimises the variability of oscillatory output in terms of the constant offset and amplitude in cells part of the population with respect to the open loop control (compare with **figure 5**, $T_f = 15000$ sec, $c = 3.0$, $\alpha = 1$). The histograms show the **(a)** constant offset and **(b)** amplitude of the cells oscillatory output, given as a percentage deviation from the homogeneous case. **(c)** Periodicity of cells in the population. **(d)** Time-series of the entire population (grey) compared with population average response (black line). In the histograms (a)-(c), the y-axis represents the number of cells and the red column illustrates the population mode. The homogeneous case, i.e. 0% heterogeneity, is given in the **supplementary figure S8**.

the constant change in population numbers, brought about by cell division and cell death, may have an effect on the performance of the chosen control strategy. To investigate any such effects we model a growing, motile, heterogeneous population that undergoes both cell division and cell death. After confirming that a population, with average doubling time of 40 minutes, can oscillate autonomously (see **figure 11**) we proceed to test the the PID-control strategy with fixed control gains ($k_p = 8.3$ min^{-1}, $k_I = 2.03E-4$ min^{-1}, $k_D = 8.3E4$ min^{-1}). The results presented earlier illustrate that the settling times of PID-control are much longer than the time required to reach a population size of 10000 cells having an average doubling time of approximately 40 minutes. As such, to identify if and when control

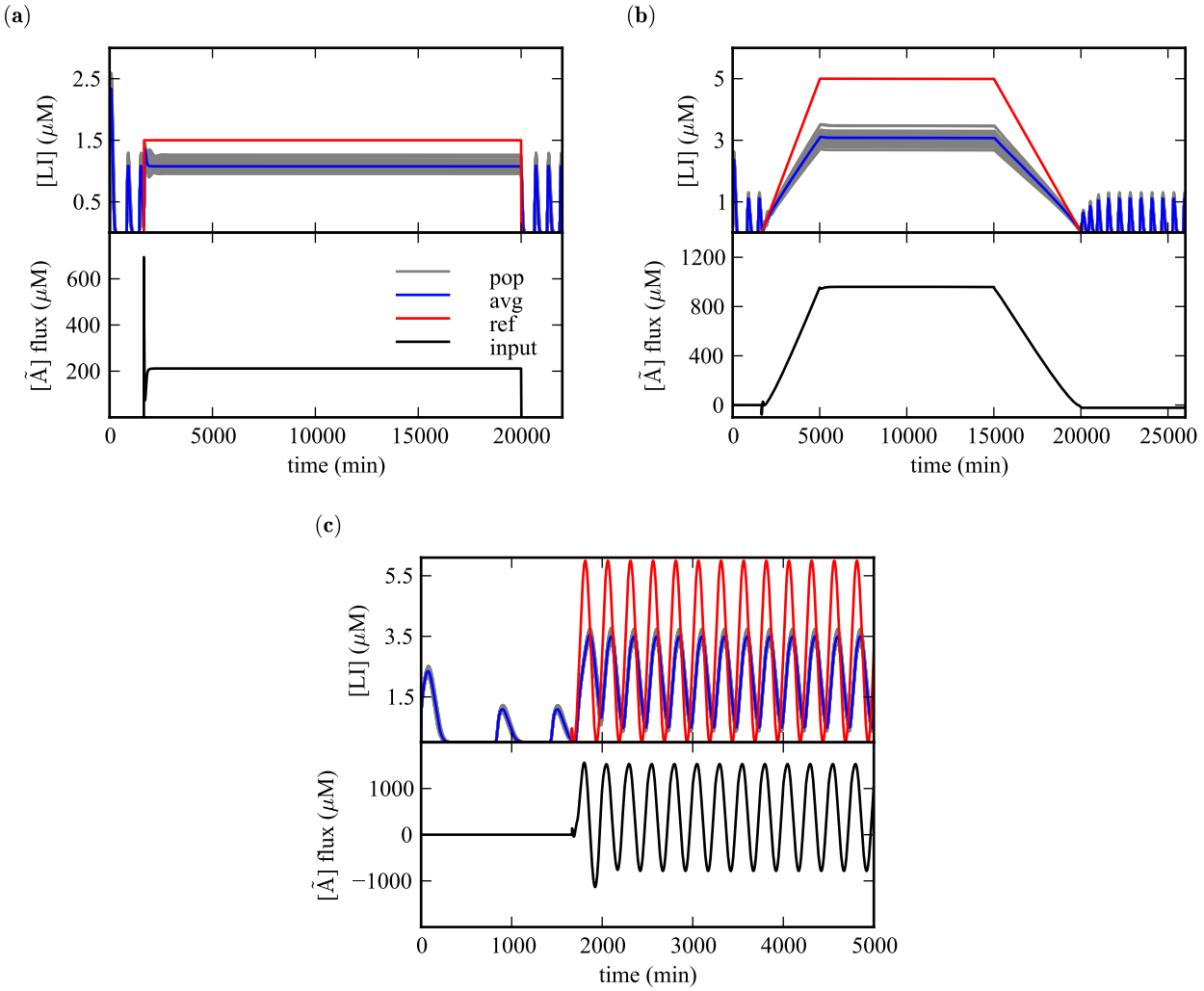

Figure 9. A heterogeneous population of 60 cells undergoing P-control. The figure illustrates time-series of a 60 cell population with 2% heterogeneity undergoing P-control ($k_p = 8.3$ min$^{-1}, c = 1.5$ μM$, t_s \approx 1660$ min$, t_e = 20000$ min). The blue line is the population average,the grey lines are the plots of all the population members and the red line is the value of the reference signal. With P-control there always remains a standard error, a difference between the reference value and the population output (here the average response). P-control allows cells to follow non-oscillatory reference signals like **(a)** fixed values ($c = 1.5$ μM) and **(b)** ramps ($y_{\min} = 0$ μM$, y_{\max} = 5$ μM) in addition to **(c)** entraining the population to a periodic input ($c = 3$ μM$, \alpha = 3, T_f = 15000$ sec) away from the natural period ($T_n = 23100$ sec). The bottom time-series in each panel indicates the control effort, the concentration of AHL required as input from the controller for each respective action.

fails we run individual simulations with different maximum population sizes, up until the 10000 cell limit.

Inspection of **figure 11** shows that our model predicts that PID-control with fixed gains can only harness a limiting population size. In all three reference-signal cases there is a reduction in the gradient of ascend of the population output with increasing population size, which indicates an increased settling time. In the case of the constant signal, there is an increasing non-smooth output with an increasing

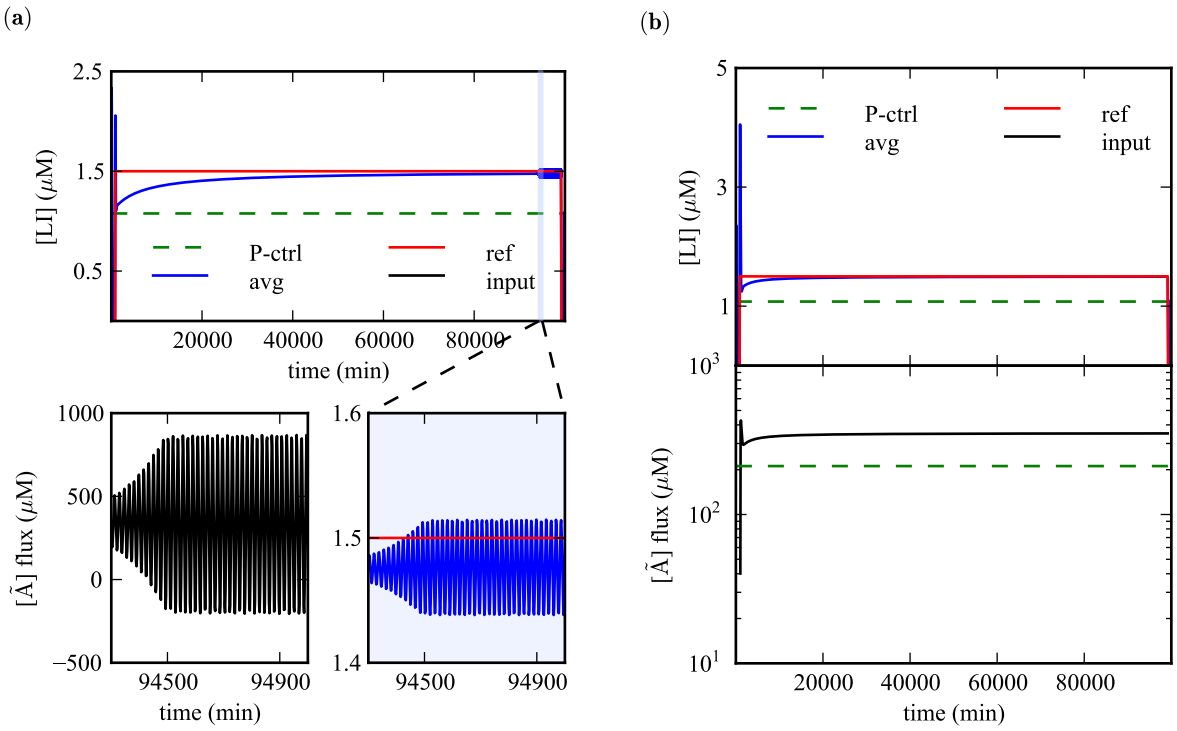

Figure 10. A heterogeneous population of 60 cells undergoing PI-control and PID-control. The figure illustrates the time-series of a 60 cell population with 2% heterogeneity. The blue line is the population average response, the red line is the value of the reference signal, $r_c(t) = 1.5$, and the dashed green line the average response of the population under proportional only control (see **figure 9 (a)**). **(a)** PI-control reduces the standard error to 1.47% of the reference value, however it does so with a slow transient. The lower panels zoom into the highlighted region of the top panel and illustrate the high frequency oscillations that can occur near the reference value and the respective chemical fluctuations of the control action during that time period ($k_p = 8.3$ min^{-1} ,$k_I = 3.97E-5$ min^{-1}, $c = 1.5$, $t_s = 833$ min, $t_e = 99166$ min). **(b)** PID-control reduces the standard error to 0.33% of the reference value. The lower panel illustrates the control effort, the amount of AHL required as input by the controller ($k_p = 8.3$ min^{-1}, $k_I = 2.03E-4$ min^{-1}, $k_D = 8.3E4$ min^{-1}).

population size whilst the signal is on. For the ramp signal, the ramp's plateau is not reached during the specified time with the ramp height diminishing whilst the population size grows. This is more pronounced in the 2500 population size scenario, where the ramp legs are indistinguishable from the ramp plateau and the population output looks parabolic instead of trapezoidal. For the oscillatory case, even though the period of the reference signal is followed there is a diminishing amplitude in the population's output as the population grows. Finally, control completely fails for population sizes beyond 2500 cells (see supplementary figure S9).

4 Discussion

As application of control over cellular populations [12–14, 16, 39] is becoming more common, we focus on investigating whether spatially resolved agent based models such as the one presented in Mina *et al.* [21] can be used to test control strategies. If so, inexpensive testing of control strategies using these models can indicate which physical implementations of control would likely be more successful and also

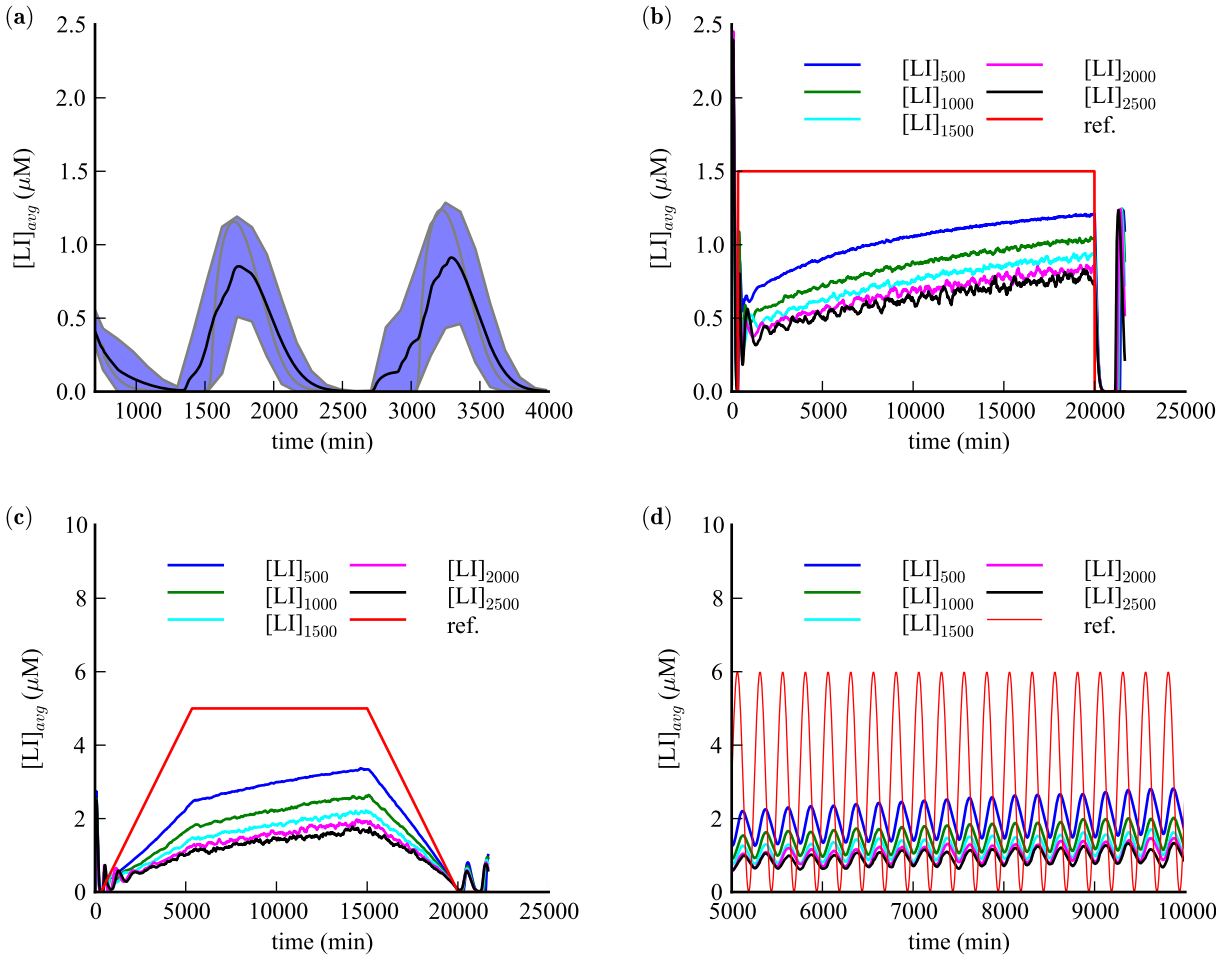

Figure 11. (a) The population average response for LI (black line illustrates the average, the blue envelope the standard deviation arising from 10 individual simulations and the grey line a typical time-series from one simulation) when there is cell division and cell death in a maximum population size of 10000 cells. **(b-d)** Time-series of a replicating population, as described in the main text, with maximum size of 500 (blue), 1000 (green), 1500 (cyan), 2000 (magenta) and 2500 (black) cells for a constant (c =1.5 μM), ramp ($y_{min} = 0$ μM, $y_{max} = 5$ μM) and oscillatory ($c = 3$ μM, $\alpha = 3$ and $T_f = 15000$ sec) reference signals respectively. It is evident that there is a degrading performance of the controller with fixed PID-control gains with an increasing population size.

give insight to the dynamic behaviours to be expected.

We adapted the spatiotemporal model presented in Mina *et al.* [21] to include open and closed loop strategies to assess if a population of oscillating cells can be entrained to a different period. We studied whether the oscillating cellular population can be forced to change dynamic behaviour by following various reference signals using linear methods of control, specifically open loop and feedback-based intervention (P-control, PI-control and PID-control), since in a physical setting these can be executed using real-time computation due to the simplicity of the underlying mathematics. We focused on studying small-sized populations in comparison to real systems in order to cover a large parameter space with our given computational power. Even so, the modelling approach presented here gives insight to the qualitative behaviour to be expected during control of the coupled population.

The open loop controller was implemented computationally by creating a sinusoidal flux of the extra-

cellular coupling chemical, Ã, through the microfluidic chamber. With increasing levels of heterogeneity, open loop control of the system resulted in loss of clustering between coupled cells as well as a diminished individual cell response in terms of amplitude (see **figure 5**). This is important as oscillatory biological mechanisms are known to operate within defined frequencies and signal strengths [43, 44] and any deviation away from these may be considered as biochemical noise and subsequently buffered from the system [31, 45]. As such, any signal obtained through control using open loop methods may be ineffective in initiating further response in the system of interest.

With open loop control, entrainment over various size populations was possible in a subset of the amplitude and forcing periods as shown in **figure 4 (b)**. Entrainment was more likely near the natural periods of the system. This is consistent with studies in linear oscillator theory [42, 46]. Analysis of the model output showed that rich periodic behaviour can be found around entrainment regions with the system changing qualitative behaviour across the entrainment boundary as shown in **figure 6** and **S4**. Unexpected periodic behaviour could be of significance in biological systems as they may have suboptimal response away from specific frequencies or amplitude thresholds [44, 47] or may result in different responses [43, 48]. For example, a system may have an additional GRN that responds to the same chemical input but only when this input illustrates a specific oscillatory waveform which may appear during open loop control and subsequently lead to unexpected behaviour.

We note that the triangular regions of entrainment stemming from $T_f/T_n \approx 1$ in **figures 4 (b)** and **S5** are reminiscent of Arnold tongues, areas of synchronisation in the (T_f, α)-plane bounded by two arcs that intersect the $\alpha = 0$ line [46]. In Arnold tongues, these arcs define a boundary of saddle-node type bifurcations [42], i.e. a change of the system from a stable to an unstable steady state. Such qualitative change of the system's behaviour across this boundary is shown in **figure S4** where phase diagrams are produced by varying the control parameter T_f. Phase diagrams of the system in the ([aA],[LI])-plane, constructed from stroboscopic sections of the system's output, illustrate the change from an unstable quasi-periodic oscillation to an attractor point in the phase plane, indicative of a stable limit cycle.

Also, according to linear oscillator theory such triangular regions of synchronisation (i.e. the Arnold tongues) appear at rational multiples of the system's natural frequency [46], here denoted as T_n, and when the forcing is not too strong. As can be seen from inspection of **figures 4 (b)** and **S5** there is also synchronisation at $T_f/T_n \approx 2$, although this does not touch the horizontal axis, i.e. when $\alpha = 0$. It is to be noted however that Arnold tongues, according to linear oscillator theory, get thinner (i.e. the arcs come closer together) as we move away from $T_f/T_n \approx 1$ [42, 46], so perhaps it is difficult to visualise in full such synchronised regions especially when using our brute-force method. Finally, we note that our system is far from linear and that we do not prove that the regions of synchronisation seen in **figures 4 (b)** and **S5** are indeed Arnold tongues. Such proof is beyond the scope of this paper but could be the subject of future work.

It would also be very interesting to confirm experimentally whether open loop control in the system creates the areas of synchronisation witnessed at integer multiples of its natural frequency, as seen through our results. Physical implementations of controller apparatus similar to the one illustrated here have been shown possible as seen in Mondragon *et al.* [39], where results also indicate synchronisation regions at multiples of the system's natural frequency. In Mondragon *et al.* [39], a population of uncoupled oscillating cells found inside a microfluidic chamber and carrying a simple activation-inhibition GRN is subject to entrainment using a sinusoidal signal. However, in Mondragon *et al.* [39] the oscillatory signal is used to induce cell behaviour and is not responsible for cell-cell coupling as with the system presented in this paper, since the cells are uncoupled. Thus in the context of our study, any physical implementation of the proposed controller should take into account that addition of extra chemicals could displace the existing chemical present in the microfluidic chamber. This can affect the total amount of autoinducer and hence disrupt cell-cell coupling. Implementation of the proposed controller should take into account such a possibility and only supplement the existing concentration of autoinducer in the microfluidic device. This could be made possible by introducing an additional device that monitors

the current concentration of extracellular AHL.

If the objective is to entrain a population to a specific periodic behaviour then a closed loop strategy is preferable as shown in **figure 7**, since open loop control is only successful in entraining the system of interest near multiples of its natural frequency, T_n. Also, the model illustrated that during open loop control cell-to-cell variability resulted in loss of clustering in the forced population as shown in **figure 5** but this level of variability was minimised for the closed loop controller as seen in **figure 8**. Furthermore, if we wish to stabilise the population around a specific value then PID-control action is preferred as it maintains a minimal standard error and allows to reach the reference value in the least amount of time (see **figures 9–10**). This is better understood when inspecting equation (14). Even though most of the control effort is contributed by P-control (see **figure 9**), a standard error is maintained between the reference value and the system's steady state [1]. A contribution to the control effort is given by the integral control term which generally eliminates the error but may cause overshooting as error correction is based on accumulation of past errors [1]. The settling time is minimised since the derivative control acts as a linear predictor for the system by estimating the rate of change of the error and contributes to minimising it based on this rate [1]. However, even with a closed loop controller one cannot control an ever growing population with fixed control gains as illustrated by the results shown in **figure 11**. This indicates the possible usage of adaptive controllers, where the control gain parameters are slowly varied/estimated from the system's input/output response in conjunction with the reference signal [49].

In conclusion, testing control methods computationally may provide insight to which physical implementations of control would likely be more successful for harnessing a biological system. Furthermore, such testing may give insight to the dynamic behaviours to be expected, such as high periodic oscillatory behaviour seen near areas of entrainment, which may cause a biological system to have undesirable output [43, 44, 47, 48]. As shown here, a breadth of responses may manifest depending on the strategy employed (e.g. open vs closed loop) and using agent based models one can quickly and inexpensively, when compared to the physical implementation of the controller, indicate the most promising strategies since both the average population response and the individual cell response may be retrieved from the model.

Acknowledgements

The authors declare no competing interests. PM was supported by EPSRC grant EP/E501214/1 and KT-A by EPSRC grant EP/I018638/1. The funders had no role in study design, data collection and analysis, decision to publish, or preparation of the manuscript. This work was carried out using the computational facilities of the Advanced Computing Research Centre, University of Bristol - http://www.bris.ac.uk/acrc/.

References

1. Aström KJ, Murray RM (2010) Feedback systems: an introduction for scientists and engineers. Princeton university press.

2. Alberts B, Johnson A, Lewis J, Raff M, Roberts K, et al. (2002) Molecular biology of the cell. Garland Science. New York. US.

3. Good LB, Sabesan S, Marsh ST, Tsakalis K, Treiman D, et al. (2009) Control of synchronization of brain dynamics leads to control of epileptic seizures in rodents. International journal of neural systems 19: 173–196.

4. Schnitzler A, Münks C, Butz M, Timmermann L, Gross J (2009) Synchronized brain network associated with essential tremor as revealed by magnetoencephalography. Movement Disorders 24: 1629–1635.

5. Hammond C, Bergman H, Brown P (2007) Pathological synchronization in parkinson's disease: networks, models and treatments. Trends in neurosciences 30: 357–364.

6. Titcombe MS, Glass L, Guehl D, Beuter A (2001) Dynamics of parkinsonian tremor during deep brain stimulation. Chaos: An Interdisciplinary Journal of Nonlinear Science 11: 766–773.

7. Xie Y, Chen L, Kang YM, Aihara K (2008) Controlling the onset of hopf bifurcation in the hodgkin-huxley model. Physical Review E 77: 061921.

8. Rusin CG, Johnson SE, Kapur J, Hudson JL (2011) Engineering the synchronization of neuron action potentials using global time-delayed feedback stimulation. Physical Review E 84: 066202.

9. Stefanatos D, Li JS (2012) Antiphase synchronization of phase-reduced oscillators using open-loop control. Physical Review E 85: 037201.

10. Batista C, Viana R, Ferrari F, Lopes S, Batista A, et al. (2013) Control of bursting synchronization in networks of hodgkin-huxley-type neurons with chemical synapses. Physical Review E 87: 042713.

11. Breslauer D, Lee P, Lee L (2006) Microfluidics-based systems biology. Mol BioSyst 2: 97–112.

12. Milias-Argeitis A, Summers S, Stewart-Ornstein J, Zuleta I, Pincus D, et al. (2011) In silico feedback for *in vivo* regulation of a gene expression circuit. Nature Biotechnology 29: 1114–1116.

13. Uhlendorf J, Miermont A, Delaveau T, Charvin G, Fages F, et al. (2012) Long-term model predictive control of gene expression at the population and single-cell levels. Proceedings of the National Academy of Sciences 109: 14271–14276.

14. Menolascina F, Di Bernardo M, Di Bernardo D (2011) Analysis, design and implementation of a novel scheme for in-vivo control of synthetic gene regulatory networks. Automatica 47: 1265–1270.

15. Cho H, Jönsson H, Campbell K, Melke P, Williams JW, et al. (2007) Self-organization in high-density bacterial colonies: efficient crowd control. PLoS Biology 5: e302.

16. Prindle A, Samayoa P, Razinkov I, Danino T, Tsimring LS, et al. (2011) A sensing array of radically coupled genetic/biopixels/'. Nature 481: 39–44.

17. Naqib F, Quail T, Musa L, Vulpe H, Nadeau J, et al. (2012) Tunable oscillations and chaotic dynamics in systems with localized synthesis. Physical Review E 85: 046210.

18. Hauptmann C, OmelChenko O, Popovych O, Maistrenko Y, Tass P (2007) Control of spatially patterned synchrony with multisite delayed feedback. Physical Review E 76: 066209.

19. Ahlborn A, Parlitz U (2008) Control and synchronization of spatiotemporal chaos. Physical Review E 77: 016201.

20. Ghosh P (2011) Control of the hopf-turing transition by time-delayed global feedback in a reaction-diffusion system. Physical Review E 84: 016222.

21. Mina P, di Bernardo M, Savery NJ, Tsaneva-Atanasova K (2013) Modelling emergence of oscillations in communicating bacteria: a structured approach from one to many cells. Journal of The Royal Society Interface 10.

22. Danino T, Mondragón-Palomino O, Tsimring L, Hasty J (2010) A synchronized quorum of genetic clocks. Nature 463: 326–330.

23. Waters CM, Bassler BL (2005) Quorum sensing: cell-to-cell communication in bacteria. Annual Review of Cell and Developmental Biology 21: 319–46.

24. Tsai TYC, Choi YS, Ma W, Pomerening JR, Tang C, et al. (2008) Robust, tunable biological oscillations from interlinked positive and negative feedback loops. Science Signalling 321: 126.

25. Novák B, Tyson JJ (2008) Design principles of biochemical oscillators. Nature Reviews Molecular Cell Biology 9: 981–991.

26. Smith H (1987) Oscillations and multiple steady states in a cyclic gene model with repression. Journal of Mathematical Biology 25: 169–190.

27. Bratsun D, Volfson D, Tsimring LS, Hasty J (2005) Delay-induced stochastic oscillations in gene regulation. Proceedings of the National Academy of Sciences of the United States of America 102: 14593–14598.

28. Müller S, Hofbauer J, Endler L, Flamm C, Widder S, et al. (2006) A generalized model of the repressilator. Journal of Mathematical Biology 53: 905–937.

29. Strelkowa N, Barahona M (2010) Switchable genetic oscillator operating in quasi-stable mode. Journal of The Royal Society Interface 7: 1071–1082.

30. Huang S (2009) Non-genetic heterogeneity of cells in development: more than just noise. Development (Cambridge, England) 136: 3853–3862.

31. Maheshri N, O'Shea EK (2007) Living with noisy genes: how cells function reliably with inherent variability in gene expression. Annu Rev Biophys Biomol Struct 36: 413–434.

32. Gorochowski T, Matyjaszkiewicz A, Todd T, Oak N, Kowalska K, et al. (2012) Bsim: An agent-based tool for modeling bacterial populations in systems and synthetic biology. PLoS One 7: e42790.

33. BSim source code [homepage on the Internet], [updated 2012; cited August 3, 2014]. Available from: `http://bsim-bccs.sourceforge.net/`.

34. Java programming language [homepage on the Internet], [updated 2013; cited August 3, 2014]. Available from: `http://java.com/`.

35. Andersen JB, Sternberg C, Poulsen LK, Bjorn SP, Givskov M, et al. (1998) New unstable variants of green fluorescent protein for studies of transient gene expression in bacteria. Applied and Environmental Microbiology 64: 2240–6.

36. Garcia-Ojalvo J, Elowitz MB, Strogatz SH (2004) Modeling a synthetic multicellular clock: repressilators coupled by quorum sensing. Proceedings of the National Academy of Sciences of the United States of America 101: 10955–10960.

37. McGinness K, Baker T (2006) Engineering controllable protein degradation. Molecular Cell : 701–07.

38. Canton B, Labno A, Endy D (2008) Refinement and standardization of synthetic biological parts and devices. Nature Biotechnology 26: 787–793.

39. Mondragón-Palomino O, Danino T, Selimkhanov J, Tsimring L, Hasty J (2011) Entrainment of a population of synthetic genetic oscillators. Science Signalling 333: 1315.

40. Alon U (2007) An introduction to systems biology. Chapman & Hall/CRC.

41. Ferry M, Razinkov I, Hasty J (2011) Microfluidics for synthetic biology from design to execution. Methods Enzymol 497: 295.

42. Stewart H, Thompson J (1986) Nonlinear dynamics and chaos. John Wiley & Sons.

43. Bootman M, Holmes A, Roderick H (2006) Calcium signalling and regulation of cell function. eLS .

44. Tsaneva-Atanasova K, Mina P, Caunt C, Armstrong S, McArdle C (2012) Decoding GnRH neurohormone pulse frequency by convergent signalling modules. Journal of The Royal Society Interface 9: 170–182.

45. Raser JM, O'Shea EK (2005) Noise in gene expression: origins, consequences, and control. Science 309: 2010–2013.

46. Pikovsky A, Rosenblum M, Kurths J (2003) Synchronization: A universal concept in nonlinear sciences, volume 12. Cambridge university press.

47. Tsaneva-Atanasova K, Caunt C, Armstrong S, Perrett R, McArdle C (2012) Decoding neurohormone pulse frequency by convergent signalling modules. Biochemical Society Transactions 40: 273.

48. Burger L, Haisenleder D, Aylor K, Marshall J (2008) Regulation of intracellular signaling cascades by GNRH pulse frequency in the rat pituitary: roles for CaMK II, ERK, and JNK activation. Biology of Reproduction 79: 947–953.

49. Åström KJ, Wittenmark B (2013) Adaptive control. Courier Dover Publications.

50. Parsek MR, Val DL, Hanzelka BL, Cronan JE, Greenberg EP (1999) Acyl homoserine-lactone quorum-sensing signal generation. Proceedings of the National Academy of Sciences of the United States of America 96: 4360–4365.

51. Schaefer AL, Val DL, Hanzelka BL, Cronan Jr JE, Greenberg E (1996) Generation of cell-to-cell signals in quorum sensing: acyl homoserine lactone synthase activity of a purified *Vibrio fischeri* LuxI protein. Proceedings of the National Academy of Sciences 93: 9505–9509.

52. Urbanowski M, Lostroh C, Greenberg E (2004) Reversible acyl-homoserine lactone binding to purified *Vibrio fischeri* LuxR protein. Journal of Bacteriology 186: 631–637.

53. Wang LH, Weng LX, Dong YH, Zhang LH (2004) Specificity and enzyme kinetics of the quorum-quenching N-acyl homoserine lactone lactonase (AHL-lactonase). Journal of Biological Chemistry 279: 13645–13651.

54. Kaplan H, Greenberg E (1985) Diffusion of autoinducer is involved in regulation of the *Vibrio fischeri* luminescence system. Microbiology 163: 1210–14.

55. Schaefer AL, Hanzelka BL, Parsek MR, Greenberg EP (2000) Detection, purification, and structural elucidation of the acyl homoserine lactone inducer of *Vibrio fischeri* luminescence and other related molecules. Methods in Enzymology 305: 288–301.

56. Wilks JC, Slonczewski JL (2007) pH of the cytoplasm and periplasm of *Escherichia coli*: rapid measurement by green fluorescent protein fluorimetry. Journal of Bacteriology 189: 5601–5607.

57. Kaufmann GF, Sartorio R, Lee SH, Rogers CJ, Meijler MM, et al. (2005) Revisiting quorum sensing: discovery of additional chemical and biological functions for 3-oxo-n-acylhomoserine lactones. Proceedings of the National Academy of Sciences of the United States of America 102: 309–314.

58. Smith C, Song H, You L (2008) Signal discrimination by differential regulation of protein stability in quorum sensing. Journal of Molecular Biology 382: 1290–1297.

59. Farrell CM, Grossman AD, Sauer RT (2005) Cytoplasmic degradation of ssrA-tagged proteins. Molecular Microbiology 57: 1750–1761.

60. Xppaut®–the differential equations tool, version 7.00; 2012, [homepage on the Internet], [updated 2012; cited August 3, 2014].

61. MATLAB (2010) version 7.10.0 (R2010a). Natick, Massachusetts: The MathWorks Inc.

Acronyms

aA acyl homoserine lactonase. 3, 4, 25

ABM agent based model. 1–3, 10, 11

AHL acyl homoserine lactone. 3, 4, 6, 7, 16, 19, 25

DDE delay differential equation. 1

GFP green fluorescent protein. 2, 6, 7

GRN genetic regulatory network. 2–6, 19

L:A LuxR:AHL complex. 3, 5, 25

LI LuxI synthase. 3, 4, 6, 25

LR LuxR, the AHL autoinducer receptor. 3

ODE ordinary differential equation. 3, 25, 26, 28

P-control proportional control. 1, 2, 9, 11, 12, 14–16, 18, 20, 26, 27, 34

PDE partial differential equation. 2, 3, 6, 25, 26, 28

PI-control proportional-integral control. 1, 2, 9, 14, 17, 18, 26, 27

PID-control proportional-integral-derivative control. 1, 2, 9, 14, 15, 17, 18, 20, 26, 27, 35

QS quorum sensing. 2

Supplementary information

All parameters, given in **table S1**, retain the same values as in Mina *et al.* [21] with the exception of the Brownian diffusion constant. The Brownian diffusion constant of AHL, $D_{\tilde{A}}$, is fixed at a value of 159 μm^{2}sec^{-1}, calculated using the Stokes-Einstein equation, $D_{\tilde{A}} = \frac{K_B T}{6\pi\eta r}$, where K_B, T, η, r are the Boltzman constant, the medium temperature, the medium viscosity and the molecule radius. We assume room temperature, $T = 298$K, and for medium viscosity we use the viscosity of water at the given room temperature, $8.90E-4$ kg.m^{-1}sec^{-2}. The molecule radius is calculated from AHL's chemical structure using an organic bond length (C-C) value of 0.154 nm resulting in an approximate molecule length of 1.54 nm.

Description (references)	Par.	Units	Value
Basal production rates			
LI [21]	a_{0_L}	μM.min^{-1}	7.79E-6
aA [21]	a_{0_A}	μM.min^{-1}	6.18E-6
Active production rates			
LI [21]	$k_{p_{LI}}$	μM.min^{-1}	9.00E-1
aA [21]	$k_{p_{aA}}$	μM.min^{-1}	9.00E-1
Cell reaction rates			
AHL production rate [50, 51]	kp_2	min^{-1}	0.90E1
LuxR AHL complex association [52]	$k_{r_{1+}}$	μM^{-1}min^{-1}	5.99E-5
LuxR AHL complex dissociation [52]	$k_{r_{1-}}$	min^{-1}	6.00E-6
AHL:aA complex catalytic rate [53]	$k_{cat_{aA}}$	min^{-1}	2.6314E3
AHL conc. adjustment for environment [54]	η_{env}	min^{-1}	3.00E-5
AHL membrane diffusion constant [22, 54]	η_{cell}	min^{-1}	0.300E1
Mean cell radius growth rate	$-$	μm.min^{-1}	3.144E-1
Michaelis-Menten constants			
L:A complex [52]	$K_{m_{LA}}$	μM	1.00E-2
aA complex [53]	$K_{m_{aA}}$	μM	1.20E3
Degradation related parameters			
L:A complex [55–57]	τ_{LA}	min^{-1}	2.40E-2
AHL [58]	$\tau_A/\tau_{\tilde{A}}$	min^{-1}	2.76E-3
Enzymatic degradation related parameters			
Inverse of $K_{M_{clx}}$ [35, 37, 59]	f	μM^{-1}	4.12E-2
$k_{cat_1} \times$ Clp$_{TOT}$ / K$_{M_{clx}}$ for LI [35, 37, 59]	δ_1	μM^{-1}min^{-1}	8.49E-1
$k_{cat_2} \times$ Clp$_{TOT}$ / K$_{M_{clx}}$ for aA [35, 37, 59]	δ_2	μM^{-1}min^{-1}	2.34E-2
Brownian diffusion			
AHL Brownian diffusion constant	$D_{\tilde{\text{A}}}$	μm^{2}sec^{-1}	1.59E2

Table S1. Values and units of parameters used in the model.

Numerical methods in BSim

BSim is a 3D framework for simulating bacterial populations [32, 33] and has numerical solvers for both ODEs and partial differential equations (PDEs). We used the Runge-Kutta order four-to-five ODE solver when solving the system of ODEs presented in equations (4)–(7). A simple finite-differences scheme is used to solve for the reaction-diffusion PDE presented in (8). Depending on the population size modelled, a time-step of 0.01 or 0.05 seconds was used and time-series data of the variables were output every 50 or 100 sec of the simulation. The bigger time-step is used when simulating the bigger

population size to reduce the computational time. The spatial aspect of the model, i.e. the $200 \times 50 \times 1$ μm^3 microfluidic chamber, was discretised into $5 \times 5 \times 1$ μm^3 elements as this was shown to be the smallest element that did not cause the finite-difference scheme to be unstable during numerical solution of the model.

To ensure that results obtained from the model are numerically correct, solutions obtained from BSim were confirmed with the numerical solutions produced from other software. Specifically, the ODE–PDE coupling was momentarily uncoupled and the numerical solution of the separate components was compared with results obtained from XPPAUT [60] and MATLAB [61]. Results obtained when solving the system of equations (4)–(7) presented in the main text in BSim using the Runge-Kutta order four-to-five ODE solver, were compared against the respective schemes of XPPAUT [60] (`Runge-Kutta`) and MATLAB [61] (`ode45`). The validity of the PDE solver was checked by introducing a fixed quantity of extracellular AHL in the environment, in the absence of cells, in order to obtain a degradation profile time-series (i.e. $\frac{\partial[\tilde{\mathrm{A}}]}{\partial t} = D_{\tilde{A}}\nabla^2[\tilde{\mathrm{A}}] - \tau_{\tilde{A}}[\tilde{\mathrm{A}}]$). This time-series was compared with results obtained when the equivalent ODE, $\frac{d[\tilde{\mathrm{A}}]}{dt} = -\tau_{\tilde{A}}[\tilde{\mathrm{A}}]$, was solved in XPPAUT [60] and MATLAB [61].

4.1 Extending BSim to include open and closed loop control

In order to implement and test the open and closed loop controllers described in the main text we added the necessary functionality to the BSim source code by (i) extending the `BSimChemicalField()` class into the `BSimChemFieldExt()` class to include methods for open loop control and (ii) creating the `ControlMethods()` and `RefSignals()` classes to allow for the implementation of closed loop control methods and reference signals, respectively, in the BSim environment. The classes are summarised in **table S2**. For clarity, in the description that follows the parameters found within the brackets of each class or method correspond to the quantities defined in the main text.

The `BSimChemFieldExt()` class inherits all methods and constructors from the chemical field class already implemented in BSim, `BSimChemicalField()`. With the `BSimChemFieldExt()` class a chemical field is constructed in the BSim environment that can be manipulated with two extra methods not available in the `BSimChemicalField()` class. The `extConstantAdd(`c`)` method is used to add a fixed amount, c, of chemical in the field at each time-step as in $r_{\mathrm{c}}(t)$ (equation (10)). The `extModSignal(`T_f, α, c, t_s`)` class is used to modify the chemical field with the sinusoidal function $r_{\sin}(t)$ (equation (11) of the main text). The amount to be added at each time-step, calculated according to the respective equations, is divided into equal parts according to the number of discretised elements of the chemical field. Then each fraction is added to each discretised element even though in experimental setups there are limited entry and exit points providing access to the chamber [11, 41], as illustrated in **figure 2** of the main text. The physical setting and our modelling implementation should not produce conflicting results since an amount added to the chamber via the controller diffuses almost instantly throughout the whole chamber as shown in **supplementary figure S2**. It is also worth noting that the external AHL spatial profile remains uniform in space throughout the autonomous oscillations of the population (i.e. in the absence of control) as illustrated in the **supplementary figure S1**.

For closed loop control, relevant methods are implemented with the `RefSignals()` and `ControlMethods()` classes. The `RefSignals()` class creates the reference signals $r_{\mathrm{c}}(t)$, $r_{\sin}(t)$ and $r_{\mathrm{rmp}}(t)$ presented in equations (10)–(12) of the main text. $r_{\mathrm{c}}(t)$ is created with the `refSignalConst(`c`)` method, $r_{\mathrm{rmp}}(t)$ with the `refSignalRamp(sim,`$y_{\mathtt{max}}, y_{\mathtt{min}}, t_s, t_1, t_2, t_e$`)` method and $r_{\sin}(t)$ with the `refSignalSin(sim,`T_f, α, c`)` method. The `ControlMethods(`k_p, ϵ, I_i, D_i`,chmfield,`t_s, t_e`)` class creates an object (where object refers to the Java technical term) that acts on the chemical field `chmfield`. The integral and derivative control gains are calculated as $k_I = k_p/I_i$ where I_i is known as the integral time and $k_D = k_p D_i$ where D_i is known as the derivative time and k_p is the P-control gain. Control can be switched off when the standard error (the difference between the target value and the current value of the system) is equal to ϵ. For these simulations we set $\epsilon = 0$. Three closed loop control methods are

available, `PIDCtrl(),PICtrl(),PCtrl()` for PID-control, PI-control and P-control respectively.

Briefly, we describe the `PIDCtrl()` method. `PIDCtrl(sim,chmfield,`$r(t)$`,avg)` adds PID-control to the simulation environment `sim` that holds the chemical field `chmfield`. The controller action is calculated accordingly for proportional, integral and derivative action from the instantaneous error $e(t)$, using the `PCtrlRtnVal(avg,`$r(t)$`)`, `ICtrlRtnVal(sim,avg,`$r(t)$`)`, `DCtrlRtnVal(sim,avg,`$r(t)$`)` methods. These methods first calculate the instantaneous error by finding the difference between the average population response `avg` and the reference value $r(t)$ where $r(t)$ can be any of the defined reference signals given in equations (10)–(12) of the main text. The amount of chemical that needs to be added or removed from the field is carried out by the `distribchem(sim,chemicalinput)` method where `chemicalinput` is the total amount calculated by the controller and retrieved using the `getchemfluxinput()` method. The adjustment is carried out by adding or removing fractions from the discretised elements of the chemical chamber as explained earlier with the `extModSignal()` method. The PI-control and P-control methods work in similar fashion taking into account their respective controller actions.

Method name	**Description**
	`BSimChemFieldExt()`
`extModSignal()`	Modulates chemical field with sin signal for open loop control.
`extConstantAdd()`	Adds constant amount of chemical into chemical field.
	`ControlMethods()`
`updateerrorlog()`	Updates vector with the standard error of the last two timesteps.
`distribchem()`	Adjusts the chemical field according to the control law action.
`PCtrlRtnVal()`	Calculates amount of chemical required according to P-control.
`ICtrlRtnVal()`	Calculates amount of chemical required according to I-control.
`DCtrlRtnVal()`	Calculates amount of chemical required according to D-control.
`PIDCtrl()`	Implements PID-control in the simulation environment.
`PICtrl()`	Implements PI-control in the simulation environment.
`PCtrl()`	Implements P-control in the simulation environment.
`getPctrlval()`	Returns the value calculated by `PCtrlRtnVal()`.
`getIctrlval()`	Returns the value calculated by `ICtrlRtnVal()`.
`getDctrlval()`	Returns the value calculated by `DCtrlRtnVal()`.
`getchemfluxinput()`	Returns the value calculated by the controller.
	`RefSignals()`
`refSignalConst()`	Creates a constant reference signal as in $r_{\mathrm{c}}(t)$.
`refSignalRamp()`	Creates a trapezoid reference signal as in $r_{\mathrm{rmp}}(t)$.
`refSignalSin()`	Creates a sinusoidal reference signal as in $r_{\mathrm{sin}}(t)$.
`getrefsignal()`	Returns the value of the reference signal at the current timestep.

Table S2. Java classes added to the BSim source code for implementing control methods. The methods have been split into the three implemented classes. The `BSimChemFieldExt()` class is for open loop control and the `ControlMethods()` and `RefSignals()` classes for closed loop control.

Assessing periodic behaviour with Poincare stroboscopic sections

The simulations were carried out in BSim, a 3D framework for simulating bacterial populations [32,33]. Depending on the population size, a time-step of 0.01 or 0.05 sec was used and time-series data of the variables were output every 50 or 100 sec of the simulation. The average response of the population was calculated during the BSim simulations based on the population size and the variables presented in the ODE equations (4)–(7) and the PDE equation (13) presented in the main text. As already mentioned, BSim uses a Runge-Kutta 45 algorithm to solve the ODEs of the intracellular dynamics and a finite difference scheme is used to solve for the chemical field PDE.

Each BSim simulation was run for a prolonged time such that transient behaviour had died out prior to assessing the periodicity of the system's output when subject to control. Post-simulation the periodic behaviour was assessed by creating a Poincare section of the average population response using the final entries of the generated time-series. The procedure is outlined below.

Depending on the length of simulation time, the last 12000-20000 entries of the output data were used. Stroboscopic sections of this truncated series were generated by assessing the average response output at multiples of the forcing period, T_f. A linear interpolator between two time-segments was used when the stroboscopic section did not coincide with a 50 or 100 sec increment. The result of this processing was the generation of a Poincare time series of the average population response at multiples of the forcing period T_f. This post-simulation processing was carried out in MATLAB [61] using custom written software.

The Poincare time-series was then assessed for periodic behaviour using MATLAB's fast fourrier transform (FFT) algorithm [61] and generating a power spectrum. If more than one frequency was present, the most powerful was selected as the one to be used in the plotting of the (α, T_f)-plane. If the strongest frequency present in the power spectrum was below a $5E-3$ threshold then the output was considered to be entrained to the forcing period.

Supplementary figures

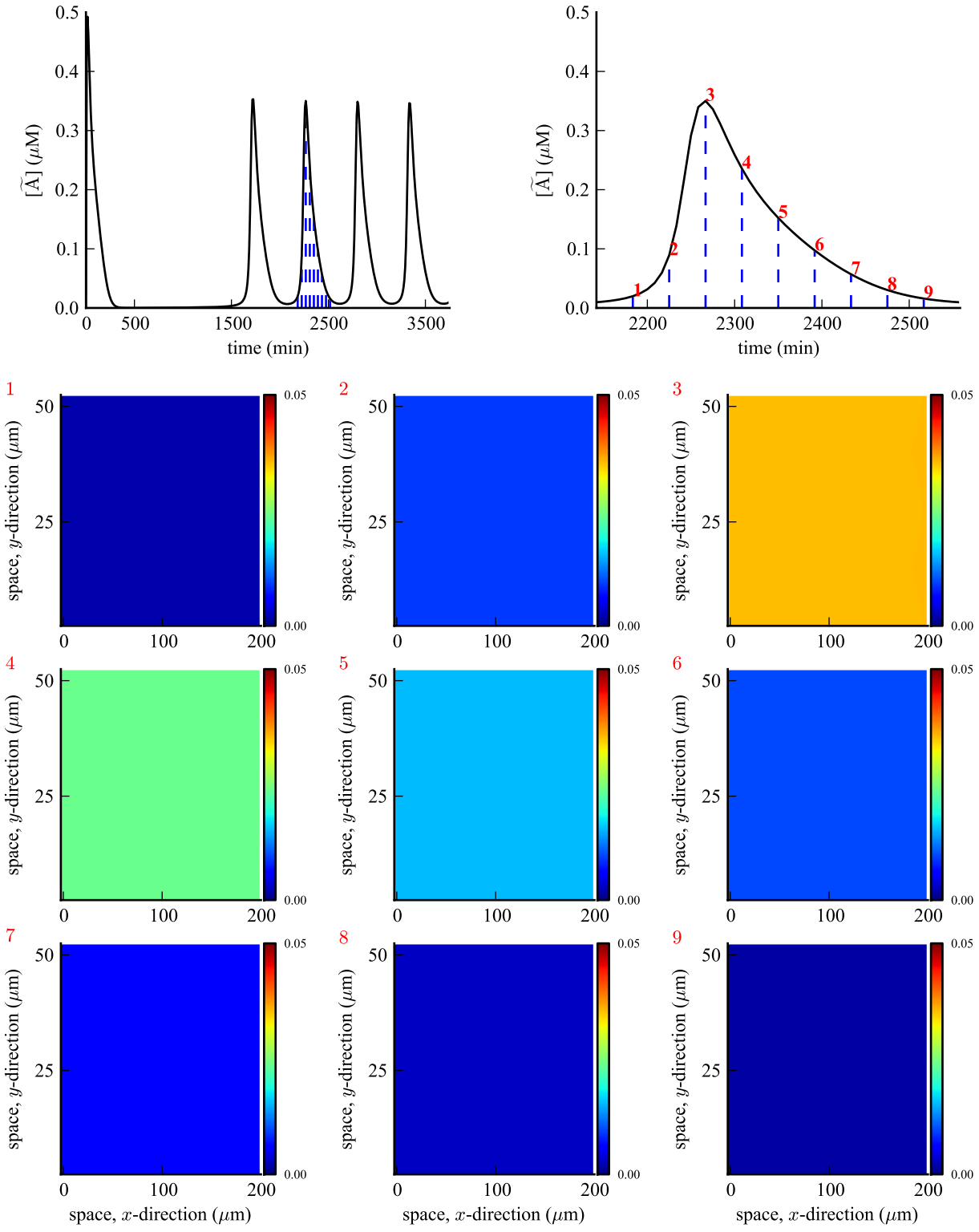

Figure S1. The spatial profile of extracellular AHL in a heterogeneous population of 10 identical cells in a $200 \times 50 \times 1$ μm^3 chamber, in the absence of control. The time-series (top row) are annotated to indicate the different time snapshots of the spatial profile of AHL that follow, when $D_{\tilde{A}} = 159$. The colorbar indicates the concentration of AHL in nanomolar (not micromolar as in the time-series). Note the uniform distribution of extracellular AHL even in the presence of a small sized population.

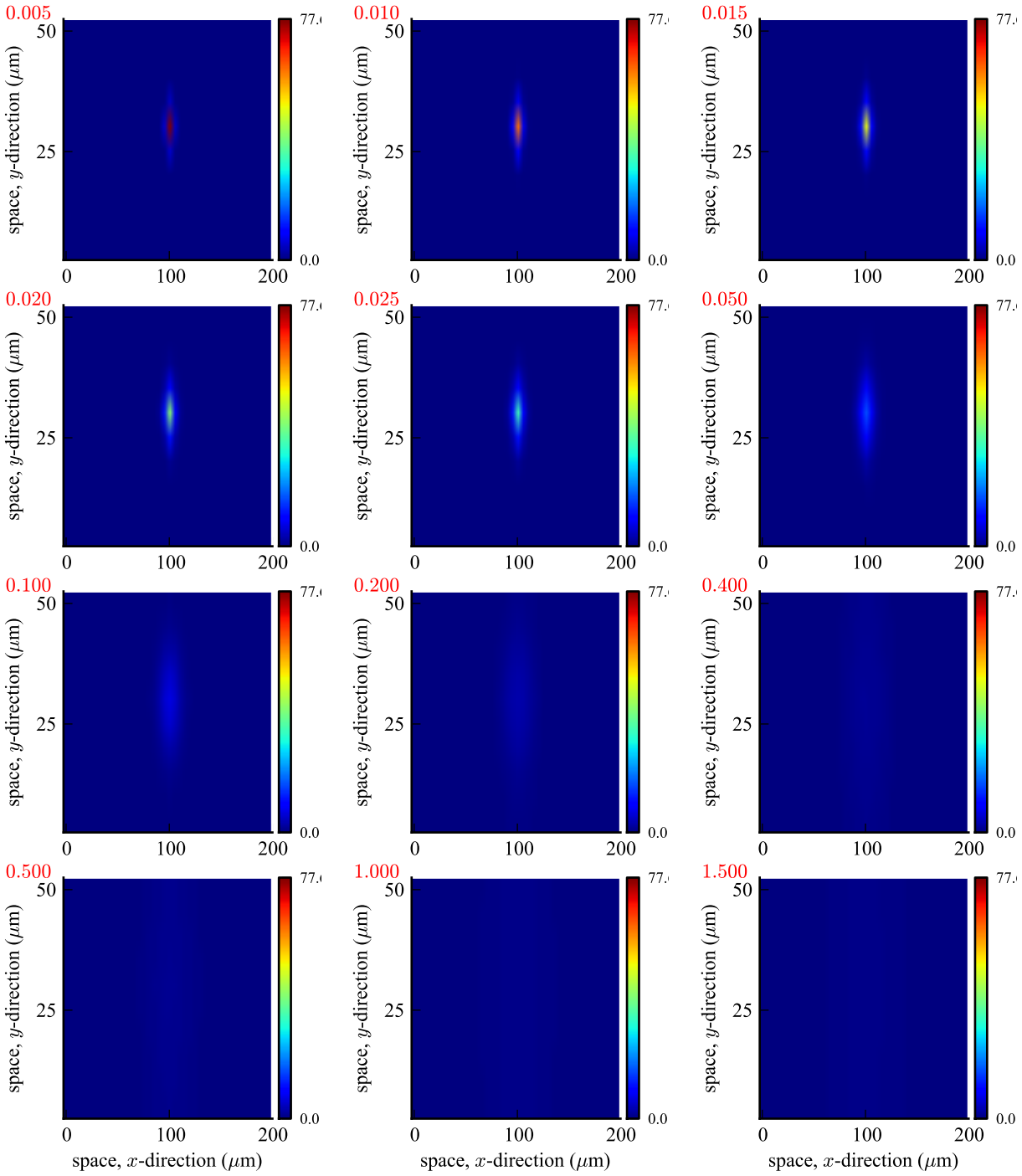

Figure S2. The spatial profile of extracellular AHL in a $200 \times 50 \times 1$ μm^3 chamber, in the absence of control and cells, when $D_{\tilde{A}} = 159$. A quantity of 2.5 μM is introduced approximately in the middle of the chamber in the absence of cells and allowed to equilibriate and degrade. Each snapshot of the spatial profile of AHL is time-stamped in seconds on the top left in red. The colorbar indicates the concentration of AHL in nanomolar. As seen the AHL equilibriates in the chamber at sub-second scale.

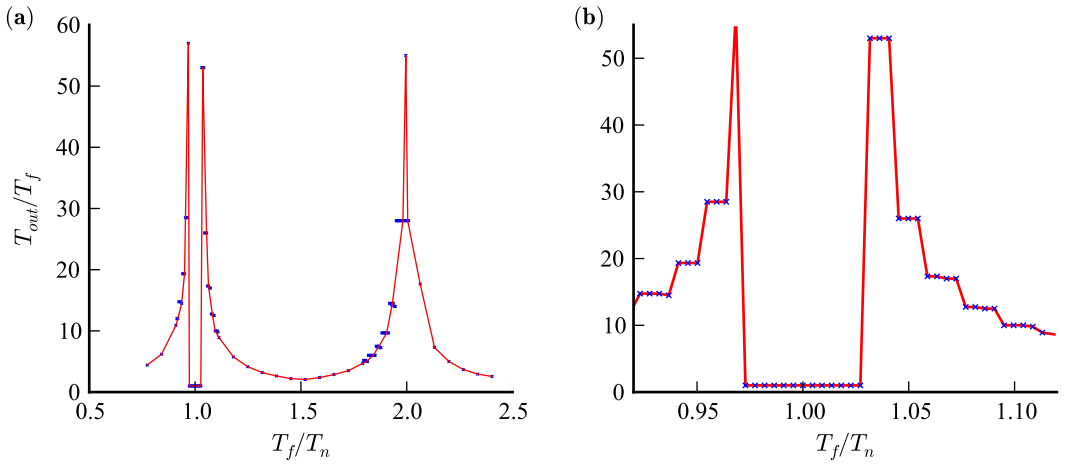

Figure S3. The population is easily entrained near its natural frequency. A small amplitude value is sufficient to entrain the population near its natural frequency during open loop control. The figure illustrates the output of open loop control when a homogeneous population of 21 cells is considered ($c = 1.0$, $\alpha = 0.2$). The range where the system is entrained is $0.97 \leq T_f/T_n \leq 1.03$. **(a)** High periodic output is seen just before and after the entrained region. High periodic behaviour is also seen at $T_f/T_n \approx 2$ but it is noted that at higher values of α the system is again entrained as illustrated **in figure 4 (b)** in the main text. Low periodic effects are also seen at $T_f/T_n \approx 1.5$. **(b)** A magnified plot around the synchronised region shows the existence of phase-slips (areas of frequency-locking followed by jumps to higher/lower periods) on either side of the synchronised area.

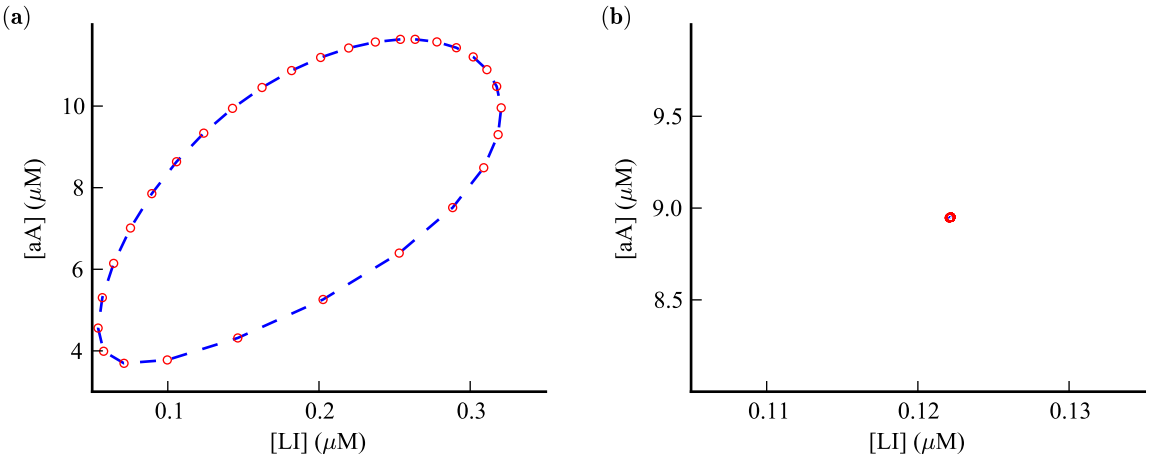

Figure S4. Projections in the ([aA],[LI])-phase plane constructed from stroboscopic sections of the average response of a 21 cell homogeneous population during open loop control. Stroboscopic sections are taken at multiples of the forcing period T_f and T_f is varied across the boundary of entrainment ($T_f/T_n = 0.96$ for **(a)** and $T_f/T_n = 0.98$ for **(b)**, $\alpha = 0.2, c = 1.0$). The maps show the transition from periodic behaviour on a torus (panel **(a)**) to a limit cycle (panel **(b)**) whilst crossing the entrainment border.

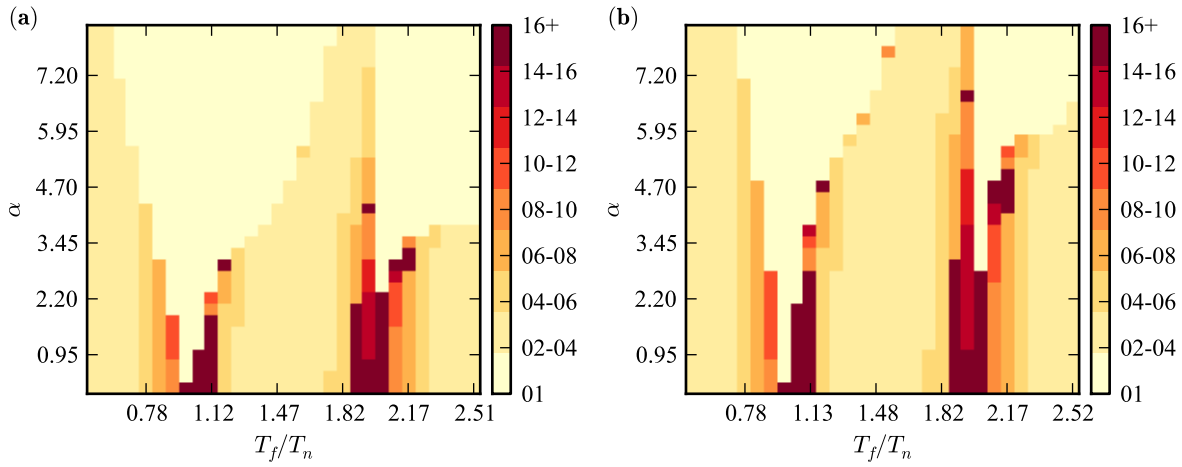

Figure S5. Average behaviour of homogeneous cell populations under open loop control. The $(\alpha, T_f/T_n)$-planes presented above show the period output of a homogeneous population that is **(a)** 60 ($c = 3.2$) and **(b)** 100 cells ($c = 5.0$) strong. As with the 21 cell strong population illustrated in **figure 4 (b)** of the main text there exist regions of entrainment when the forcing period is near the population's natural period, $T_f/T_n \approx 1$ and $T_f/T_n \approx 1$.

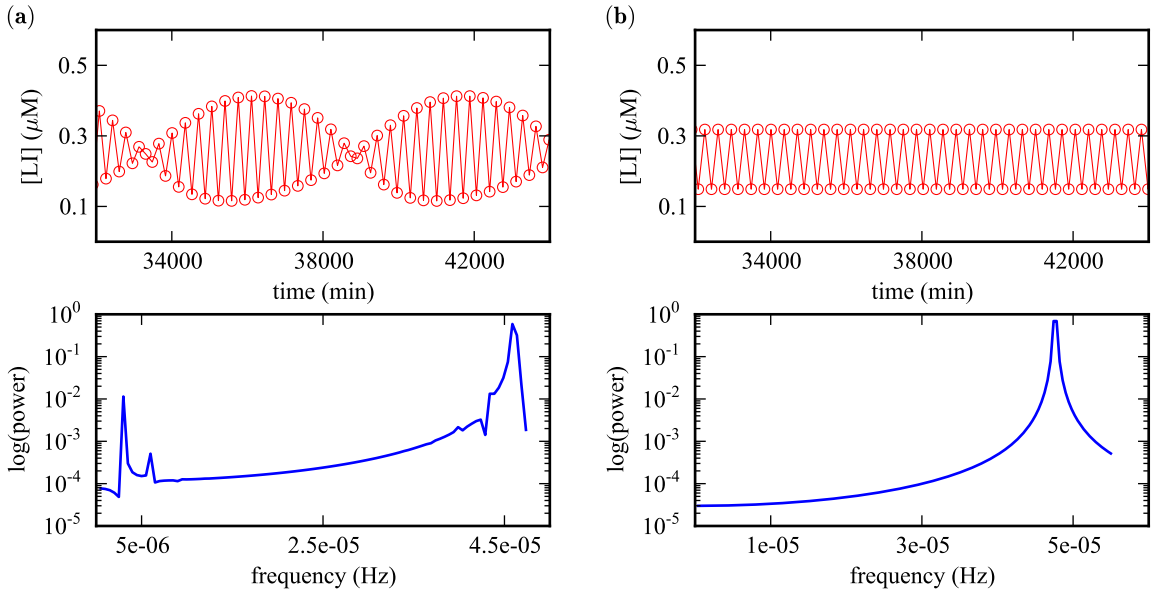

Figure S6. Stroboscopic sections and power spectrums of a 60-cell heterogeneous population. The figure illustrates stroboscopic sections and power spectrums of annotated points 1 and 6 as presented in **figure 6** of the main text. Point 1 is shown in **(a)** where the behaviour is governed by two separate frequencies as shown by the two big peaks of the power spectrum. As the amplitude of the forcing is increased only the small period remains (panel **(b)**).

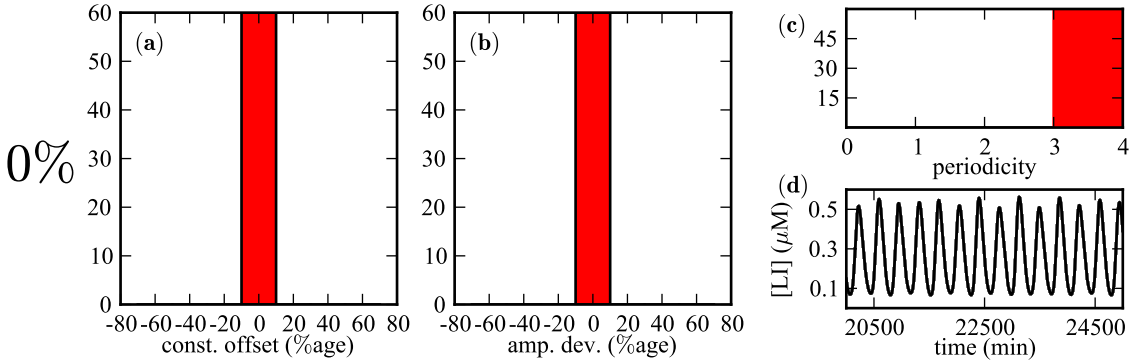

Figure S7. Histograms of a homogenous population (i.e. 0% heterogeneity) undergoing open loop control. In panels **(a)** constant offset and **(b)** amplitude of cells part of the population, are given as a percentage deviation from the homogeneous case. In panel **(c)** the periodicity of cells in the population is given. In panel **(d)** the time-series of the entire population (grey) is compared with the population average response (black line). In the histograms (a)-(c), the y-axis represents the number of cells and the red column illustrates the population mode. ($T_f = 15000$ sec, $c = 3.0$, $\alpha = 1.0$)

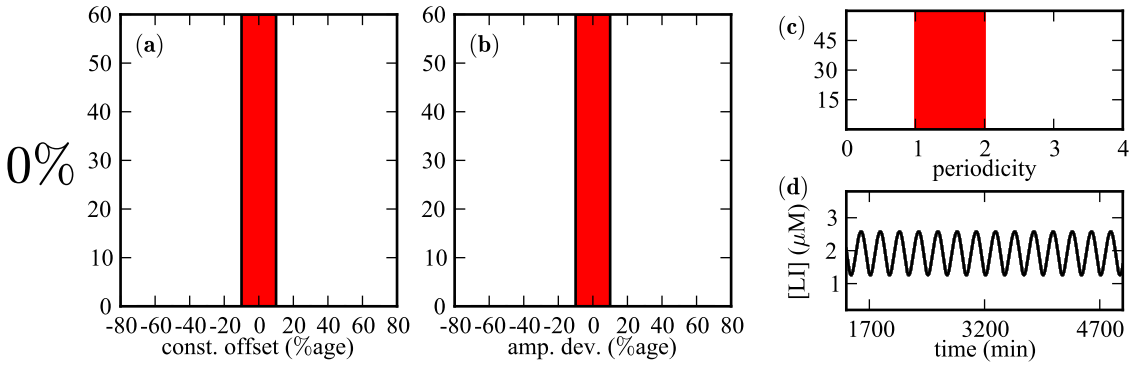

Figure S8. Histograms of a homogenous population (i.e. 0% heterogeneity) undergoing P-control. In panels **(a)** constant offset and **(b)** amplitude of cells part of the population, are given as a percentage deviation from the homogeneous case. In panel **(c)** the periodicity of cells in the population is given. In panel **(d)** the time-series of the entire population (grey) is compared with the population average response (black line). In the histograms (a)-(c), the y-axis represents the number of cells and the red column illustrates the population mode. ($T_f = 15000$ sec, $c = 3.0$, $\alpha = 1$)

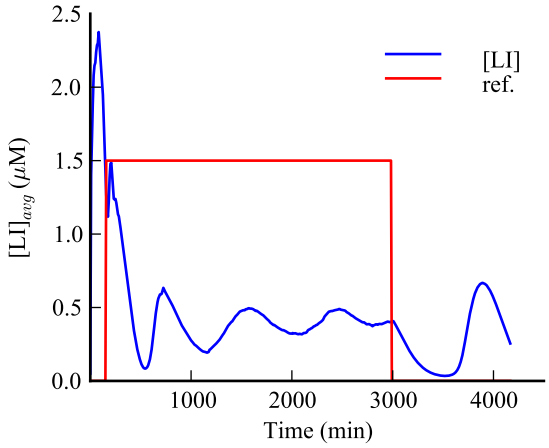

Figure S9. An example of PID-control control for a population size of 3000 cells with a constant reference signal ($c = 1.5$). The control fails in regulating the population for tracking the reference signal.